

**Microstructural and mineralogical analysis of greenschist-facies deformation
in the eastern Yukon-Tanana terrane, Yukon, Canada**

Cassis Lindsay

lindsc1@mcmaster.ca

April 15, 2022

McMaster University

Abstract

The Yukon-Tanana terrane of the northern Canadian Cordillera experienced multiple episodes of mafic-intermediate volcanism during the Paleozoic, followed by polyphase deformation during its accretion to the North American continent. This study seeks to analyse the deformation history of a heterolithic greenschist unit that is exposed near the Boswell River in south-central Yukon. This greenschist unit, which is coincident with an aeromagnetic high, includes thinly layered intervals that exhibit centimeter to meter-scale folds and crenulations.

Using an oriented greenschist facies sample collected from a meter-scale fold during field mapping, a detailed microstructural approach was applied to determine the number and nature of deformation events recorded in the area. Subsequent petrographic analysis was conducted to identify the minerals present and establish the temperature during deformation. Observations show that the main mineral phases are quartz-muscovite-chlorite, in addition to a variety of sulphide minerals, some of which show compositional zonation. A fracture runs through the slide, bearing crushed mica along one border, possibly indicative of shear. Based on these observations, it was established that the sample records at least three distinct stages of deformation. To further constrain the deformation history, use of a scanning electron microscope (SEM) was employed to link the observations to the larger-scale tectonic evolution of the area.

Acknowledgements

Many thanks to my undergraduate supervisor, Dr. Alexander Peace (McMaster University), and my field supervisor, Dr. David Moynihan (Yukon Geological Survey) for their guidance and support during this project, from beginning to end, and to Dr. Heidi Daxberger (University of Toronto) for the composite slide scans that allowed me to work remotely in the fall. I would also like to acknowledge the Yukon Geological Survey for enabling and assisting with this undergraduate thesis, Marcia Reid with the Canadian Center for Electron Microscopy for SEM training, and the Stereonet 11 software.

Table of Contents

Abstract.....	1
Acknowledgements	1
Table of Contents	2
List of Figures.....	3
Introduction.....	4
1. Geological Setting.....	5
1.1 Canadian Cordillera	8
1.2 Yukon Tanana Terrane	9
1.3 Deformation	10
1.4 Study Area	10
2. Methodologies.....	11
2.1 Sample Collection & Preparation	12
2.2 Petrographic Microscope.....	14
2.3 Scanning Electron Microscope.....	14
3. Results	16
3.1 Petrology.....	16
3.2 Microstructural Data	17
3.3 SEM Elemental Analysis	21
4. Discussion	21
4.1 Mineralogy	21
4.2 Evolution	22
Conclusions.....	24
References	26
Appendix A.....	29

Appendix B 33

List of Figures

Figure 1: Regional Study Area. 5

Figure 2: Geological Map. 6

Figure 3: Evolution of the YTT. 8

Figure 4: Sample Location. 12

Figure 5: Sample outcrop. 13

Figure 6: Sample Preparation. 14

Figure 7: Half-Slide Scan 15

Figure 8: Qtz-Mus-Chl. 16

Figure 9: Pyx-Cal. 17

Figure 10: Pyrite Zoning. 18

Figure 11: Pyx-Mica Feature 18

Figure 12: Calcite Twins. 19

Figure 13: Mineral Alteration..... 19

Figure 14: Stereonet..... 20

Figure 15: Fracture..... 20

Introduction

Before the late 1990's, the Yukon Tanana terrane (YTT) had been debated regarding evolution, stages, and types of deformation (Parsons et al., 2022) despite decades of research like that of Templeman-Kluit (1976), Churkin et al. (1982), and Hansen (1989). After 1997, a spike of activity in the YTT led to a significant increase in radiometric dating, mapping, and related projects (Nelson et al., 2006). Consequently, the boundaries, and many of the assemblages within the YTT, were redefined and the literature was summarized by Nelson et al. (2006). This study will examine a sample, taken from a greenschist fold in the Boswell River region in the Big Salmon Range, and determine how many episodes of deformation or alteration occurred by examining the mineralogy and microstructures. In addition, we will attempt to identify what type of environment led to the formation of the sample. Observations and analysis of the sample will be completed with the use of a petrographic and scanning electron microscope (SEM). The aim of this work is to analyse the sample and compare our findings to previous work from the region. In particular, to compare our findings to the ages and lithologies of Moynihan et al. (2022), and the deformation described in Stevens and Erdmer (1996) and Mihalynuk (1997). Knowledge of the surroundings is important to understand larger scale structures and patterns. Therefore, it will be interesting to compare the results of our outcrop to prior literature. This study will add to the documentation in the area on the small scale, by close analysis of a sample from a folded outcrop observed during the field period. The findings of this study could help with further mapping and discovery in the region since there is raw mineralogical data at this point. Prior to Moynihan et al. (2022), mapping of the Big Salmon Range had been at a less detailed 1:250,000 scale (Templeman-Kluit, 1984), and several earlier maps from Cockfield et al. (1936), Lees (1936), and Mulligan (1963). Stevens (1997) mapped at a more detailed 1:50,000 scale, relatively recently, in 1994. The mineralogy will detail the mineral assemblages and identify whether dateable zircon grains are present to provide an age for the outcrop. Having data at this outcrop will assist in future mapping, which will in turn lead to available data for the public to access. This could influence further terrane evolution studies in the region, in addition to geological exploration in the Big Salmon Range.

1. Geological Setting

The area of interest, shown in Figure 1, is situated in south-central Yukon Territory, at the north end of the Canadian Cordillera, in the mountains of the Big Salmon Range. Located northeast of Whitehorse, Yukon, the area is north of the city of Teslin and bounded on the west by the Teslin River. A geological map from Moynihan et al. (2022) depicts the simplified geology and geological successions within the mapping area as shown in Figure 2. The South Big Salmon River runs to the north of the sample area and flows into Quiet Lake, which borders the southeast. This region is where the YTT accreted onto North America during the Late Triassic (Hansen, 1989). A map of the terranes is shown in Figure 1. Terranes are fault-bounded

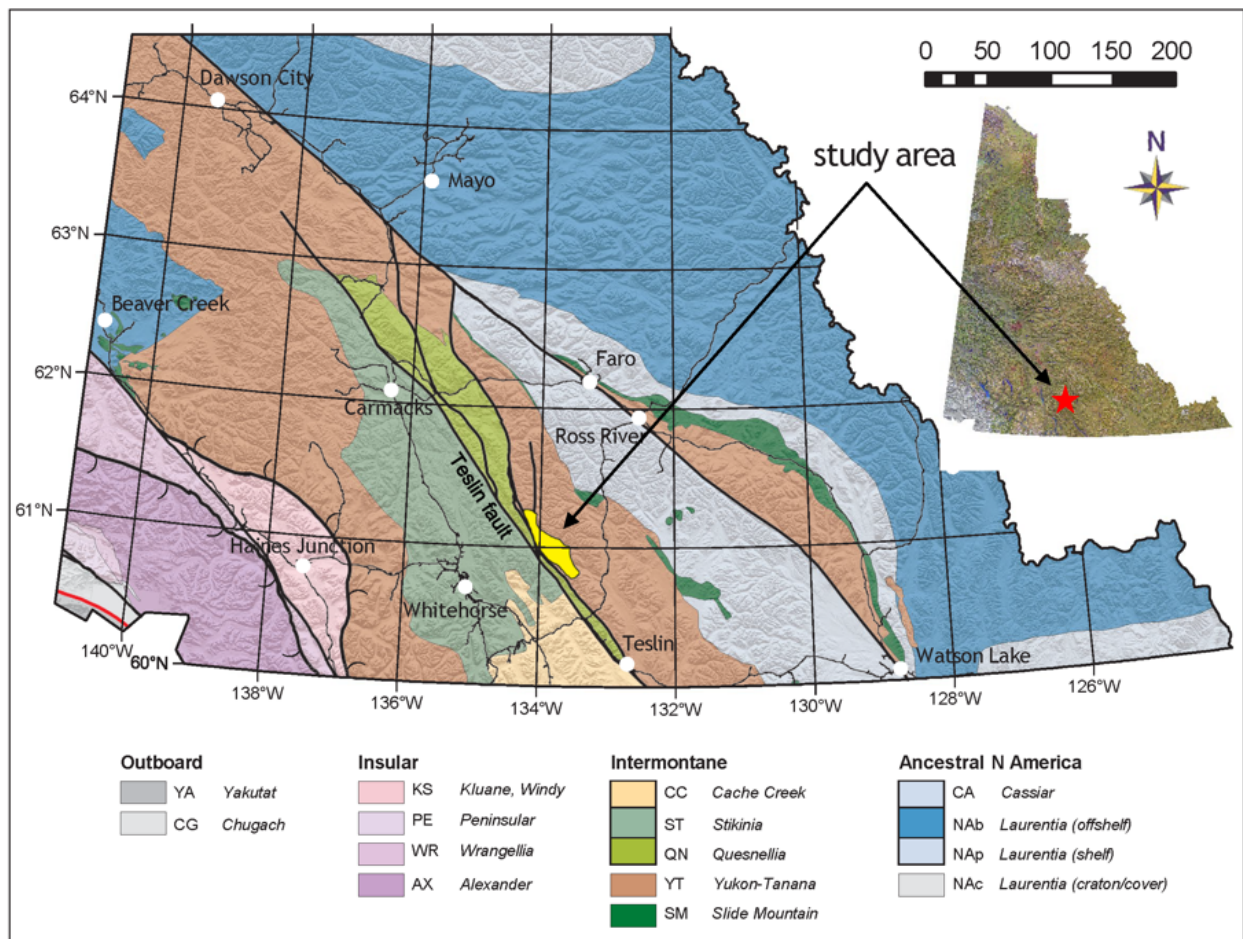


Figure 1. Study area depicted. Terrane map from Moynihan et al. (2022), showing study area outlined in yellow. This same location can be seen in the inset map to the right, showing the region in reference to the Yukon Territory. Study area is within the YTT, bordered to the west by the Teslin fault. Stikinia terrane is west of the Teslin fault and the study area; Quesnellia terrane is located just east of the Teslin fault and follows the length of the fault beyond the extent of our study location.

lithospheric entities with distinct internal stratigraphy with respect to one another and the North American craton (de Keijzer, 2002). The study area with distinct deformation, was recently mapped, with preliminary observations from Moynihan et al. (2022) outlining the geology of the major units and supplementing age estimates with new U-Pb data. This was the first time this region had been mapped at a detailed scale since Stevens in 1994.

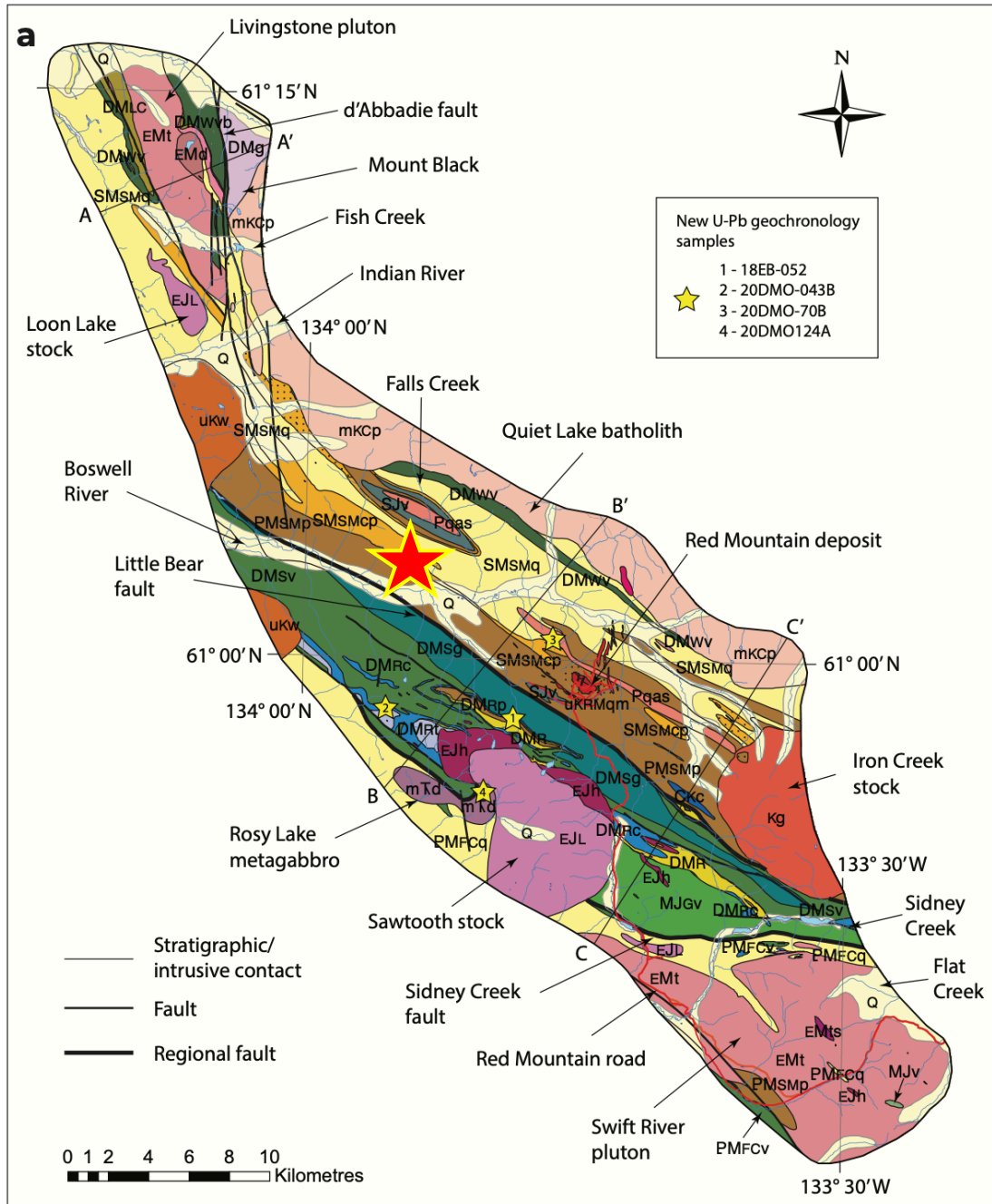


Figure 2. (a) Simplified geological map taken from Moynihan et al. (2022), showing the mapping area. Our sample is from the red starred location, northeast of the Little Bear fault and north of the Boswell River. **(b)** Legend (below).

b**Legend****Quaternary**

 Q *Unconsolidated glacial, glaciofluvial and glaciallacustrine sediments; fluvial silt, sand and gravel deposits; volcanic ash; partly covered by soil and organic deposits*

INTRUSIVE ROCKS**Cretaceous**

 uKRMqm *altered porphyritic quartz monzonite with abundant sheeted quartz veins; host to Red Mtn. Mo deposit*

 mKcP *porphyritic to megacrystic biotite granite*

 Kd *porphyritic (plagioclase, biotite) dacite*

 Kg *muscovite-biotite granite, leucogranite; mostly equigranular*

Triassic-Jurassic

 EJh *hornblende, hornblende-biotite pegmatite*

 EJL *granodiorite, local hornblende*

 mTd *Rosy Lake metagabbro: metagabbro, metadiorite*

Permian

 Pqas *quartz and feldspar augen schist*

Devonian-Mississippian

 EMg *metagranodiorite with abundant white mica, epidote*

 EMts *schistose metatonalite; micaceous, garnet-bearing*

 DMg *porphyritic biotite granite with abundant K-spar 'augen'*

 EMd *metadiorite, quartz diorite, hornblende; lesser metatonalite*

 EMlt *leucotonalite, commonly contains sparsely-distributed amphibole pseudomorphs*

 EMt *hornblende-bearing tonalite, leucotonalite, quartz diorite, diorite. Includes minor quartzite, greenschist and metasedimentary schist*

METASEDIMENTARY, METAVOLCANIC AND VOLCANIC ROCKS**Cretaceous**

 uKw *rhyolite, dacite*

Paleozoic-Mesozoic

 SJv *greenschist, locally with siliceous layers; finely layered greenschist*

 MJv *mafic breccia, amphibole-biotite schist*

Carboniferous (Klinkit assemblage)

 CKc *coral-rich limestone; calcite and dolomite marble*

Gunsight succession

 MJGv *lapilli tuff, block tuff, ash tuff, sandstone, siltstone*

Rosy succession

 DMR *interlayered metachert and calc-schist/tuff; graphitic phyllite, greenschist, calc-silicate and marble*

 DMrt *metachert; grey, pale brown, green or pink*

 DMRp *graphitic phyllite*

 DMRv *greenschist; minty-green chlorite schist with amphibole phenocrysts; lapilli tuff, green volcanoclastic sandstone*

 DMRc *grey and cream marble; calc-silicate*

Sawtooth succession

 DMSg *metagabbro, greenschist; minor leucogabbro*

 DMSvc *pale green, thinly layered volcanoclastic rocks; variably siliceous chlorite-muscovite schist; minor marble*

 DMSv *greenschist; lesser metagabbro*

Livingstone Creek succession (Finlayson assemblage)

 DMLC *calc-schist, greenschist, micaceous schist, quartzite/metachert*

 DMLCq *dolomitic quartzite*

Wiley succession (Finlayson assemblage)

 DMWc *marble, calc-silicate schist*

 DMWtc *tuffaceous carbonate, amphibole schist*

 DMWvb *compositionally banded greenschist; lapilli tuff*

 DMWv *greenschist; includes intervals of compositionally banded greenschist and lapilli tuff*

Slate Mountain succession (Snowcap and/or Finlayson assemblages)

 SMSMq *quartzite and micaceous quartzite, lesser calc-silicate and marble, minor greenschist*

 SMSMm *grey weathering, white marble and calc-silicate*

 SMSMcp *calc-phyllite and schist, commonly chlorite-rich, calcareous quartzite, graphitic phyllite*

 SMSMCS *green, coarse grained amphibole-bearing calc-silicate*

 PMSmt *black quartzite (metachert?)*

 PMSMp *graphitic phyllite, minor quartzite*

 PMSMph *hornfelsed graphitic phyllite, minor quartzite*

Flat Creek succession (Snowcap and/or Finlayson assemblages)

 PMFCv *metabasalt*

 PMFCm *marble, calc-silicate*

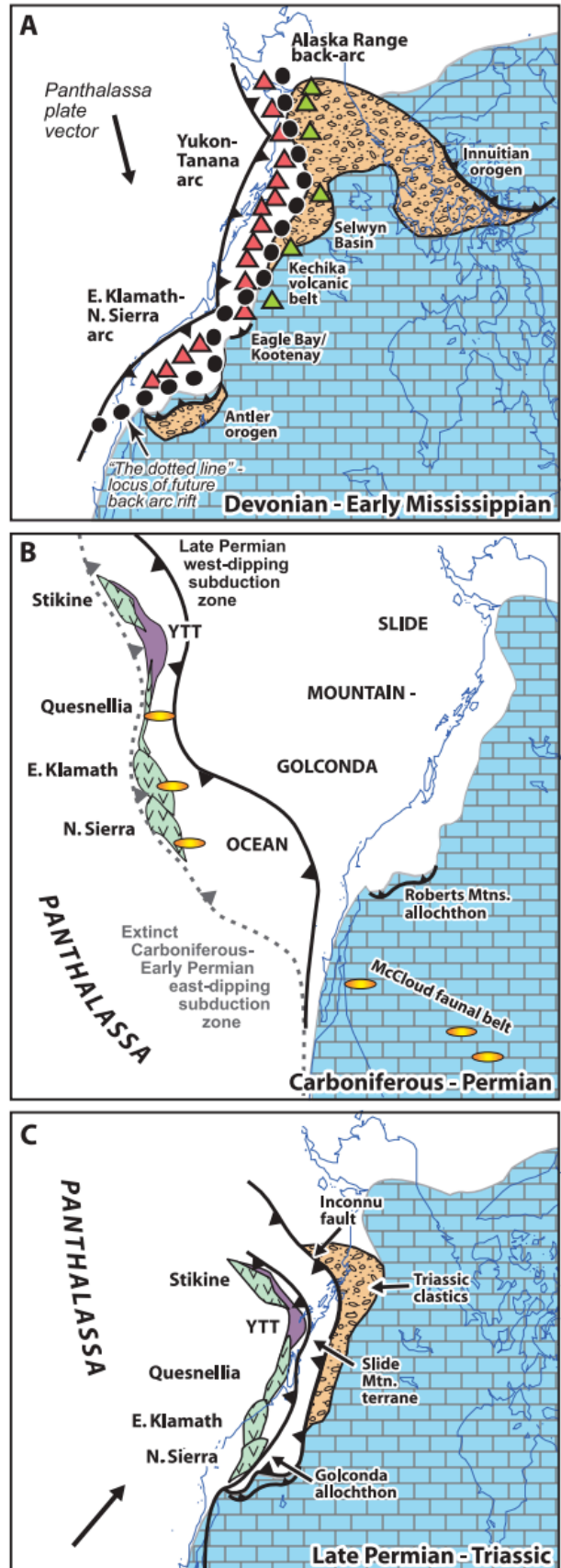
 PMFCq *micaceous quartzite, quartzite, local grit*

 PMFCp *graphitic phyllite, schist, minor quartzite*

1.1 Canadian Cordillera

The northern reach of the Canadian Cordillera stretches into the Yukon Territory. Simard et al. (2003) states that the Cordillera is considered to be a collage of allochthonous oceanic and pericratonic terranes which accreted onto ancestral North America at various points during the Mesozoic era. Figure 3 shows a possible accretionary scenario for the intermontane terranes. These terranes are separated into groups classified by shared geodynamic scenarios (Colpron et al., 2007): Intermontane, Insular, Northern Alaska, and Late Accreted. The intermontane terranes are described to be peri-cratonic and are differentiated from the other groups by their

Figure 3. Evolution of the Northern Cordillera intermontane terranes (taken from Colpron et al., 2007). The Yukon-Tanana terrane is shown in purple, labeled as YTT. Ancestral North America is the landmass coloured blue. The outline of the modern coastline, including the tail of Alaska and Vancouver Island, can be seen. Our sample would have been part of the Yukon-Tanana arc in this diagram. **(A)** Shows the development of volcanic arcs at a subduction zone, including the Yukon-Tanana arc, during the Devonian-Early Mississippian. **(B)** Depicts the south-western movement of the terranes during the opening of the Slide Mountain basin to the North during the Carboniferous-Permian. In **(C)**, the Slide Mountain basin closes, causing the YTT to move northeast in the Late Permian-Triassic, closer toward the continent where it would eventually accrete.



evolution in the mid- to late-Paleozoic era, in the peri-Laurentian realm (Colpron et al., 2007). The intermontane terranes that extend into the Yukon are limited to the Cache Creek, Stikinia, Quesnellia, Yukon-Tanana, and Slide Mountain terranes (Colpron et al., 2007). The YTT borders ancestral North America, to the east of other accreted terranes like the insular, coast, and other intermontane terranes (Ruks et al., 2006).

1.2 Yukon Tanana Terrane

Previous work has described the YTT as an extensive metamorphic-plutonic assemblage of variably deformed ductile tectonites (Hansen et al., 1991). It represents a broad band of metamorphic rocks that stretches from Alaska into the Yukon, between the Denali and Tintina faults (Hansen et al., 1991) pictured on Figure 1, and comprises of four assemblages: the Snowcap, Finlayson, Klinkit, and Klondike (Moynihan et al., 2022). Hansen et al. (1991) historically suggested that the YTT could be divided into 5 assemblages, including the Nisutlin, Anvil, and three granitoid assemblages based on lithology and crystallization age. Murphy et al. (2006) and Simard et al. (2003) agree that YTT evolved in an arc or back-arc setting, but Simard et al. (2003) goes further to suggest that the YTT evolved from an outboard strip of continental crust that the volcanic arc formed on. Simard et al. (2003) also suggests that the volcano-sedimentary assemblages of the YTT basement could represent pieces of a single late Paleozoic arc system that was dismembered prior to accretion onto ancestral North America. Moynihan et al. (2022) agrees with the arc environment that developed the metavolcanic, metasedimentary and metaplutonic rocks during the middle to late Paleozoic. Moynihan et al. (2022) adds that the Proterozoic-Devonian metasedimentary rocks are interpreted to have been rifted from the Laurentian margin, a group now called the Snowcap assemblage. Murphy et al. (2006) details early events in the evolution of the YTT, describing three fault-bounded successions of Upper Devonian-Lower-Mississippian metavolcanic and metaplutonic rocks that were deposited on a pre-Late Devonian ensialic basement in west or south-west facing forearc, arc and back-arc settings. The terrane was then imbricated by north to northeast vergent thrust faults in the Early Permian, followed by the halting of Upper Triassic sedimentary rock deposition due to the closing of the Slide Mountain basin in the Middle Permian (Murphy et al., 2006). Simard et al. (2003) suggested that the YTT is equivalent to the basement of the Quesnel terrane and could be the northern extension of the Quesnel terrane, due to the variably metamorphosed sedimentary and volcanic successions with abundant dioritic to granitic intrusions of dominantly

Mississippian age. However, YTT can be differentiated from the surrounding terranes by patterns of penetrative ductile deformation fabric (Hansen et al., 1991) and because Quesnel and Stikine are intra-oceanic terranes (Simard et al., 2003).

1.3 Deformation

The YTT underwent polyphase deformation, but the history and ages of this ductile deformation are not clearly defined, leading to confusion (Hansen et al., 1991). Mihalynuk et al. (2006) identified four phases of deformation, with the oldest evidence being relicts of amphibolite grade porphyroblasts, followed by a stage of orogeny deformation, regional transposition fabric potentially related to a Late Permian collision event (Fig. 3), and folding correlated to a rapid uplift event related to collision with the northern continental margin. A belt of polydeformed sedimentary and submarine volcanic rocks that extend up into the Yukon from British-Columbia is called the Big Salmon Complex (Mihalynuk et al., 2006). This was previously interpreted as the Teslin Tectonic Zone or the Teslin Suture Zone. Hansen et al. (1991) also identified four ductile deformation events, some overlapping, which include Early Jurassic preaccretion deformation, Early Jurassic to Mid-Cretaceous Synaccretion deformation, Mid-Cretaceous Crustal Extension, and Mid- to Late- Cretaceous Strike-Slip Translation and Plutonism. Hansen et al. (1991) notes that the Late Triassic/Early Jurassic granitoids and intrusions postdate predominantly the ductile deformation of their host rocks. Moynihan et al. (2022) found that all pre-Jurassic rocks in the region are deformed, with some Early Jurassic intrusions showing signs of minor deformation, meaning they likely intruded during the weakening stage of deformation. In addition, the study region hosts largely undeformed Cretaceous intrusions (Moynihan et al., 2022).

1.4 Study Area

The freshly mapped area in the Big Salmon Range within the YTT has been split into three structural domains based on the Little Bear and Sidney Creek faults, both regional-scale discontinuities (Moynihan et al., 2022). This area is centered around the Boswell River, shown in Figure 2, and is part of the northeastern division, above the Little Bear fault. This division comprises of metasedimentary, mafic and volcanoclastic rocks (Moynihan et al., 2022). The lithology to the northeastern side of the Little Bear fault is dominated by a metasedimentary unit, the Slate Mountain succession (Moynihan et al., 2022). The region between the Little Bear fault and the Sidney Creek fault is dominated by greenschist and metagabbro, with some

metasedimentary rocks (Moynihan et al., 2022). Below the Sidney Creek fault, the area is dominated by intermediate Mississippian metaplutonic and older metasedimentary rocks. The Big Salmon strike-slip fault cuts through to the west at a northeast-southwest direction and the d'Abbadie fault system sits to the east, both post-accretionary faults (de Keijzer et al., 1999). The d'Abbadie fault system has multiple stages of ductile fabrics, with younger brittle structures (Colpron, 2005). The Big Salmon River valley contains multiple high-angle faults trending NNW, including the Teslin Fault (Hansen, 1989). Moynihan et al. (2022) list the various assemblages, successions, and suites appearing within this region. The assemblages include the Boswell, Finlayson, Klinkit, Klondike, and the Snowcap, although there may be some overlap between the Snowcap and Finlayson assemblages (Moynihan et al., 2022). The successions are the Slate Mountain, Wiley, Livingstone Creek, Sawtooth, Rosy, Gunsight, and the Flat Creek (Moynihan et al., 2022). The Finlayson assemblage contains the Livingstone Creek succession of calc-schist, greenschist, micaceous schist, quartzite/metachert, and dolomitic quartzite (Moynihan et al., 2022). It also contains the Wiley succession of marble calc-silicate schist, tuffaceous carbonate, amphibole schist, compositionally banded greenschist, and lapilli tuff (Moynihan et al., 2022). Units within the Slate Mountain succession and the Flat Creek succession may belong to either the Finlayson or Snowcap assemblage (Moynihan et al., 2022). The Klinkit assemblage contains Carboniferous rocks, like coral-rich limestone, calcite and dolomite marble (Moynihan et al., 2022). The relationship between the successions and assemblages can be seen in Figure 2. The suites include the Early Mississippian Simpson Range suite intrusions, Jurassic Lokken suite, the Late Devonian-Early Mississippian Grass Lakes suite, the Late Cretaceous Red Mountain suite, and the Mississippian Tatmain or Kelly suite (Moynihan et al., 2022).

2. Methodologies

This section will describe the preparation and procedure involved with the sample, from collection in the field to lab analysis. Two methods of analysis were conducted in the space of three months. The sample was located and extracted from south-central Yukon Territory, in the Big Salmon Range, by Little Bear Mountain. This region is approximately 72 kilometers northeast from Whitehorse and is shown in Figure 4.

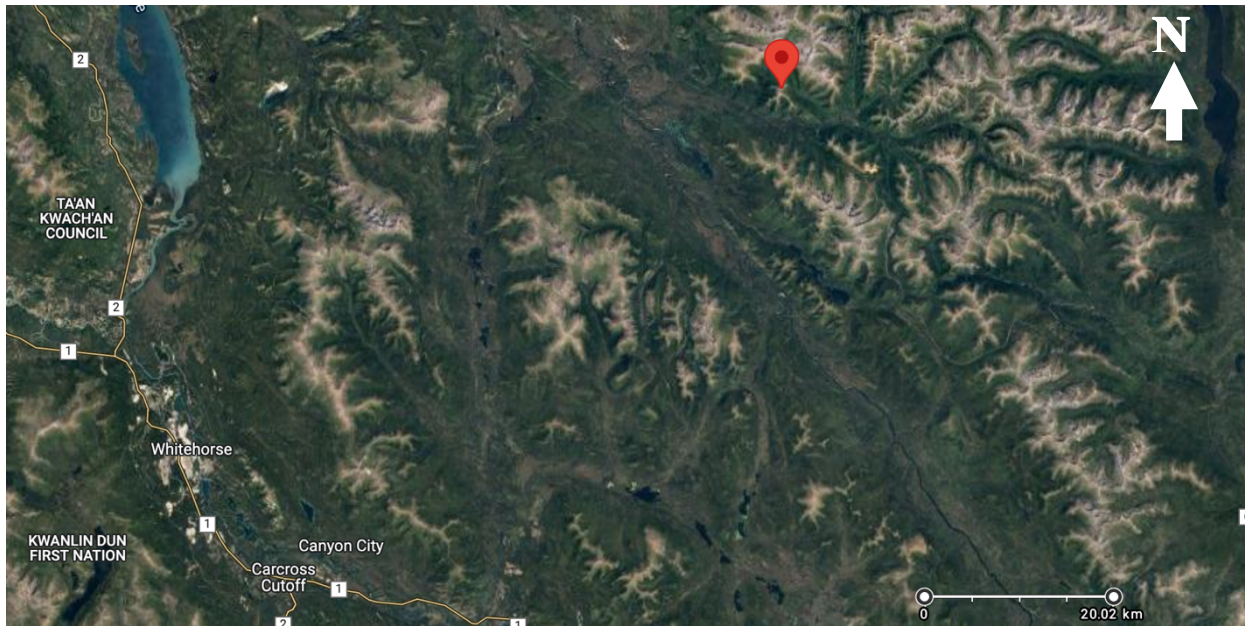


Figure 4. Closer look at sample location, with reference to Whitehorse, Yukon.

2.1 Sample Collection & Preparation

The orientated sample was collected in the field from outcrop, as shown in Figure 5a. The sample was taken at $61^{\circ}03'54.3''\text{N}$ $133^{\circ}54'47.9''\text{W}$, shown by red marker on the map in Figure 4, taken from Google Maps. The outcrop displayed centimeter to meter scale concentric folding and thin layers, which were green and white to the eye and can be seen in Figure 5b. The sample was chosen for ease of removal while keeping it intact. This was important to conserve the orientation and the integrity of the folds and structures within. Once transported from the field, it was cut into multiple pieces using an oil saw (Fig. 6), epoxied for durability, and prepared for shipping at the Yukon Geological Survey office. After being mailed to McMaster University, a piece was cut. The area was selected due to strategic presence of both visible mineral-type bands, a fold axis, and clear metallic grains. The cut piece was larger than the conventional thin section size, as one large thin section was desired. It would be simpler to examine one large slide rather than switch between two smaller slides. The selection was sent to Precision Petrographics Ltd., in Vancouver, BC, where it was turned into a 5 cm by 3.5 cm thin section. Before the SEM was used, the thin section was carbon coated.

Figure 5. (a) Sample was taken from concentrically folded greenschist outcrop. Direction looking south.
(b) Exposed fold surface with green micaceous layers and white layers visible within part of the fold. Not sampled. Rusty mineral alteration visible. Lineations were observed on the fold surface. Pen and hammer for scale.





Figure 6. Sample resting in oil saw after being cut at the Yukon Geological Survey office. Arrows on left image show lineations on fold surface. Layer differentiation can be observed on the cut face.

2.2 Petrographic Microscope

A petrographic microscope at McMaster University was used to analyse the sample in both plain polarized light (PPL) and cross polarized light (XPL). Specifically, a Nikon Ci-POL polarizing microscope was used. The mineralogy and textures were systematically recorded, with emphasis on identifying the dominant mineral phases. A full-slide scan in both PPL and XPL was conducted by Dr. Heidi Daxberger at University of Toronto Scarborough, capturing the entire slide in 4 compositive images, two in PPL, and the other two in XPL. One of these images can be found on the following page in Figure 7. These images can be found in greater detail in Appendix A.

2.3 Scanning Electron Microscope

The polished sample was viewed in a Tescan Vega II LSU SEM (Tescan USA, PA) operating at 20kV. This is a similar method to Chakrabarti et al. (2013), except our study used a slightly higher kV for a better resolution, where the 2013 paper detailed using 15kV. The SEM was equipped with an Oxford X-Max 80 Energy Dispersive Spectroscopy detector and Inca software (Oxford Instruments, UK) from which spectra and weight percentages were obtained with working distance to the detector set at 15mm. Spectral Analysis was carried out on certain grains using backscattered electrons (BSE). The standard for calibration is a polished nickel wafer with 99.99% purity. Spectral analysis allowed for an elemental composition summary of



Figure 7. Half-slide scan in XPL. XPL was chosen to display the difference in minerals to a greater degree than in PPL. Notice the fracture at the top and the folding pattern evident on the scan.

selected points on grains. The microscope was mainly used to observe the relationship between the minerals, and gain elemental peak data, following the methods from the literature of Humayun et al. (2013) and Tomomewo et al. (2019). Once again, our study used higher kV than Humayun et al. (2013) for higher resolution and differentiation between similar minerals. The SEM backscatter electron (BSE) view shows grains with elements higher up the periodic table as brighter relative to surrounding minerals. Both the Chakrabarti et al. (2013) and Humayun et al. (2013) studies focused on BSE, like this research, but only Humayun et al., were analysing a full slide. Chakrabarti et al. (2013) were focusing on single grains within their slide, but the method for both studies was similar.

3. Results

This section details the results of the mineralogy from petrographic analysis, as well as the elemental data from use of the SEM. Rock textures, minerals, their relationships and structures are described in this section. In the hand sample, the fold showed layers ranging from millimetres to 8 centimeters height, with both white and green micaceous layers, some of which can be observed in the cut sample in Figure 6. Lineations were observed on the exposed surfaces.

3.1 Petrology

The sample consists mainly of intermingled quartz, of fairly constant grain size, and mica, with clusters of different, larger grains, and metallic grains dispersed throughout. The mica varies in length greatly throughout. The quartz grains measure approximately 100 micrometers in diameter throughout the slide, on average. These grains show undulate extinction in XPL, and all grains show no signs of fractures or cleavage. They are generally round or oval, but noticeably lengthen along one axis at different places within the fabric of the fold and display low first order birefringence in greys and whites. The micas, both muscovite and chlorite, are long, thin grains, with a feathery habit. The muscovite shows third-order birefringence, while the chlorite stays mostly dark grey/extinct. The muscovite grains are colourless in PPL, while the chlorite shows colourless-to-green pleochroism. Figure 8 shows the combination of quartz and the micas. The clusters of larger grains consist of two main types: the first being a euhedral, long and rectangular grain showing second-order birefringence colours, and the second group being clusters of somewhat-altered, semi-euhedral grains displaying twinning that remains obvious in both PPL and XPL. The former grains are slightly green polychroic, with fractures running

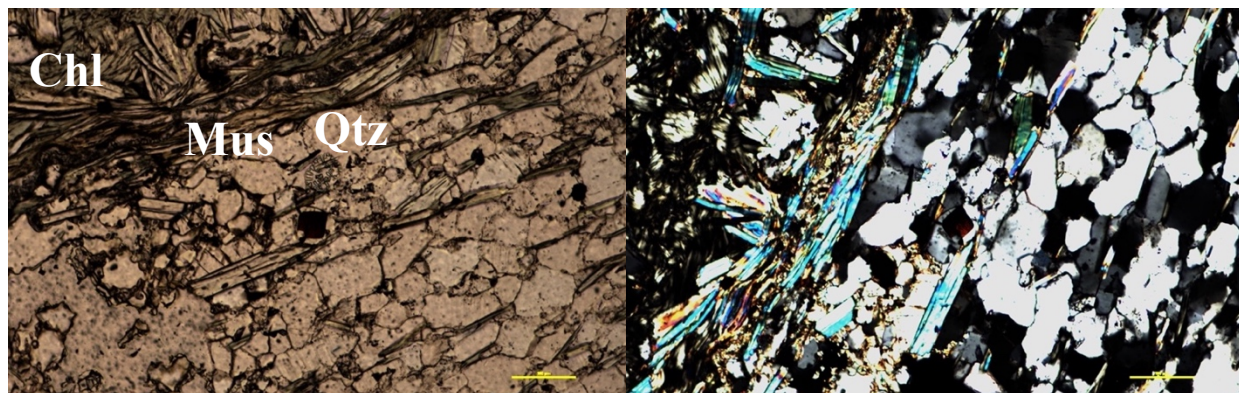


Figure 8. Mica (chlorite = Chl, muscovite = Mus) and rounded quartz (Qtz) grains in PPL (left) and XPL (right), showing the banding of mica and also a mix of the two mineral groups. The XPL image was rotated slightly to capture the right extinction angles. Scale says 100 micrometers (Mu).

perpendicular to the long axis of the grain. They are less prevalent than the second group of larger minerals, with only 4 individual grains identified in the slide. Average grain length was 450 micrometers. The second group of grains show first order birefringence colours, with many grains showing mineral alteration. These grains are colourless in PPL and show cleavage at approximately 75 degrees. The grain size varies but is on average up to 10 times larger than the quartz grains, with an estimated average of 600 micrometers. These two grains are shown briefly in Figure 9, but in greater details in section 3.2. The interspersed metallic grains are smaller than the larger grain clusters, but still larger than most individual quartz grains. Some form groups that are visible to the naked eye on the polished surface of the sample. They are cubic and/or triangular in shape, with most displaying compositional zonation visible under petrographic microscope and SEM. The inner zone tends to be darker than the outer border, as shown in Figure 10. These grains are isotropic in XPL and opaque in PPL, although some show blotches of red colouring in both PPL and XPL.

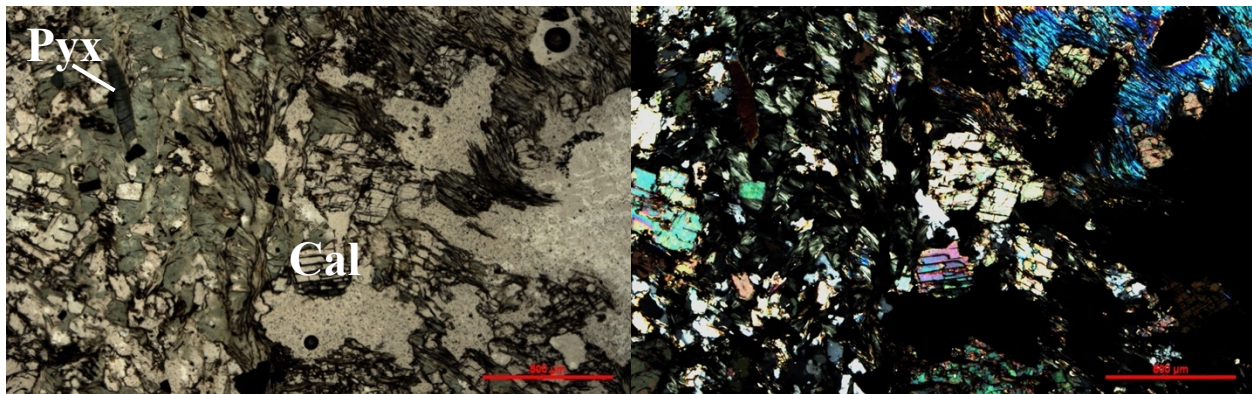


Figure 9. Pyroxene (Pyx) and Calcite (Cal) shown in PPL (left) and XPL (right). Image was chosen to show proximity between the mineral types; these two minerals were found near each other throughout the slide. Scale says 500 micrometers (Mu).

3.2 Microstructural Data

The sample is differentiated into bands of quartz and micas following the pattern of the folds. It is a medium-coarse-grained rock, with schistose foliation, zoned by bands of quartz and micas. The groundmass seen in between spaces in the quartz-mica fabric is too fine to identify. The micas are tightly spaced with the quartz and have undergone deformation, as kinking is evident in many areas on the thin section (Figure 11). The quartz grains continuously show undulatory extinction (Fig. 8). Another indicator of deformation in the quartz are the elongated grains at

some parts in the thin section, demonstrated to some degree in Figure 8, where the quartz grains closest to the muscovite are relatively elongated. Within the quartz-mica zones, there are clusters of larger grains which is where most empty spaces occur. Whether this is a natural occurrence or the result of thin section preparation could not be definitively determined. Some of the larger grains with high relief also show twinning (Figure 12). These are calcite grains that show thin (< 1 micron) and thick tabular deformation twins (> 5 microns) (Ferrill et al., 2004). Twinning is not apparent on every calcite grain. There is a rust-colored, fine-grained mass that is found throughout the sample and is also visible to the naked eye. This rust often appears when a mineral, usually calcite, seems to be altered, and has been observed to overprint an existing mineral, as seen in Figure 13. The texture is quite grainy and appears more cohesive under BSE SEM analysis. The overall foliation direction can be seen in the full-slide scans, partially shown in Figure 7. Field measurements of cleavage and fold axis planes were collected, and are shown by stereonet

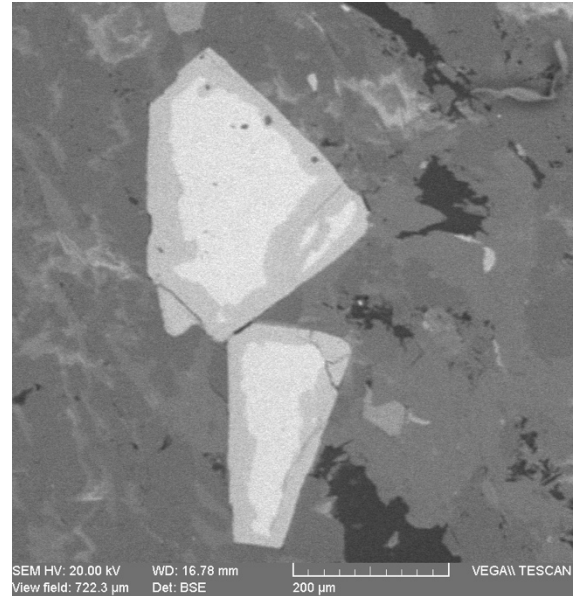


Figure 10. Pyrite grain showing compositional zonation on a SEM BSE image.

Figure 11. Pyroxene (Pyx) grain cross-cutting muscovite kinking in PPL (top) and XPL (bottom)



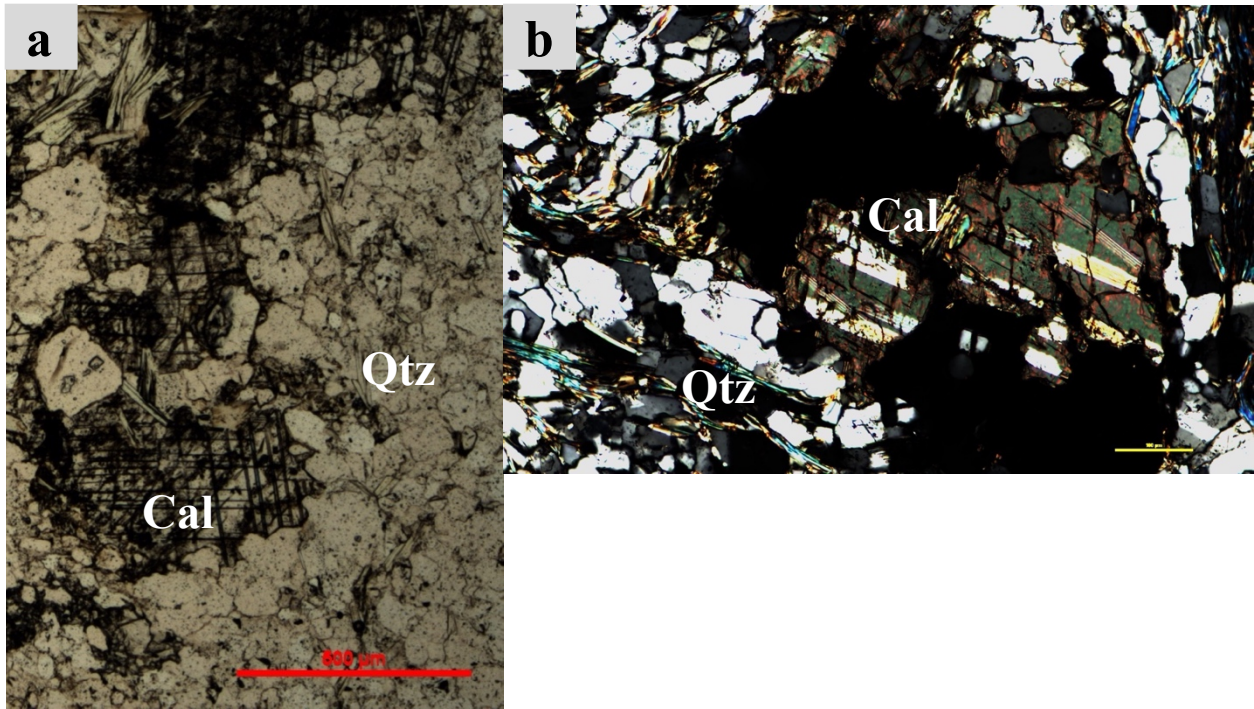


Figure 12. Examples of calcite (Cal) twinning in two different images. **(a)** Thin pleochroic twins in PPL. Scale says 500 Mu. **(b)** thick tabular twins in XPL. Scale says 100 Mu.

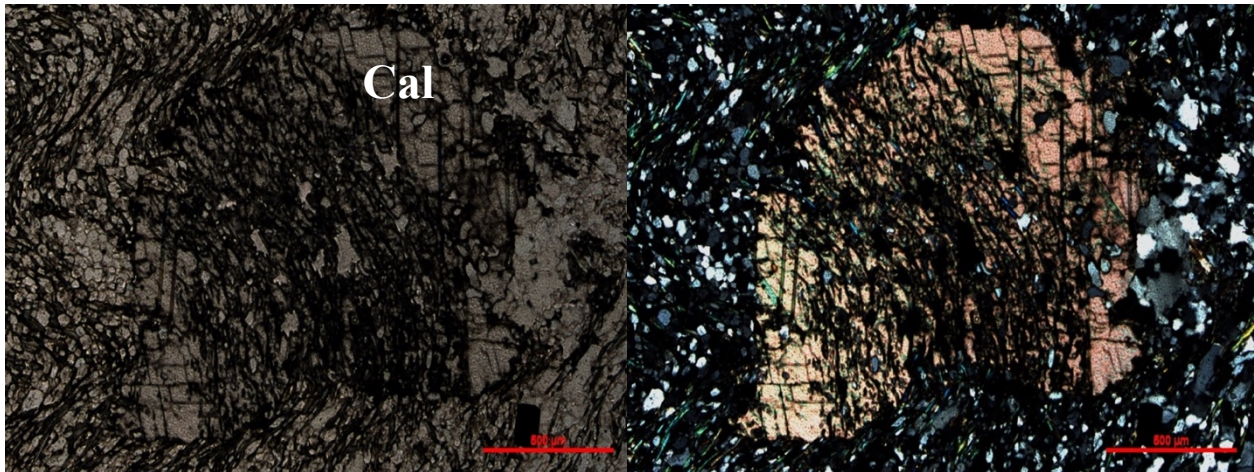


Figure 13. Alteration of larger calcite (Cal) grain by rust-colored fine-grained mineral. Groundmass of finer grained quartz and some mica. Seen in PPL (left) and XPL (right). Scale says 500 Mu.

in Figure 14, using Stereonet 11 software. The angle between planes is 38.8° or 141.2° . The thin section showed a fracture running down the center of the slide. This was the most obvious feature, with sheared micas along only one border of the fracture, as seen in Figure 15. The fracture ranged from 150-250 micrometers in width, and the inside of the fracture contained

Figure 14. Stereonet showing measurements of cleavage and fold axis planes.

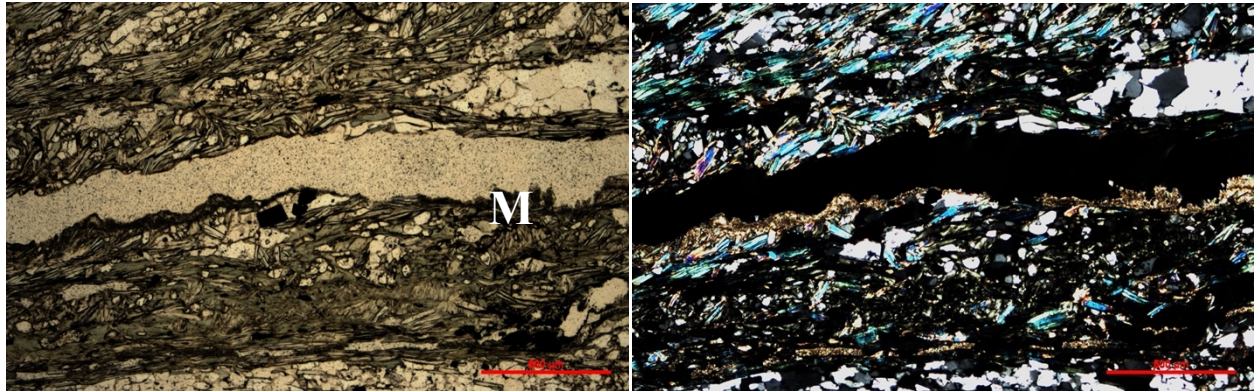
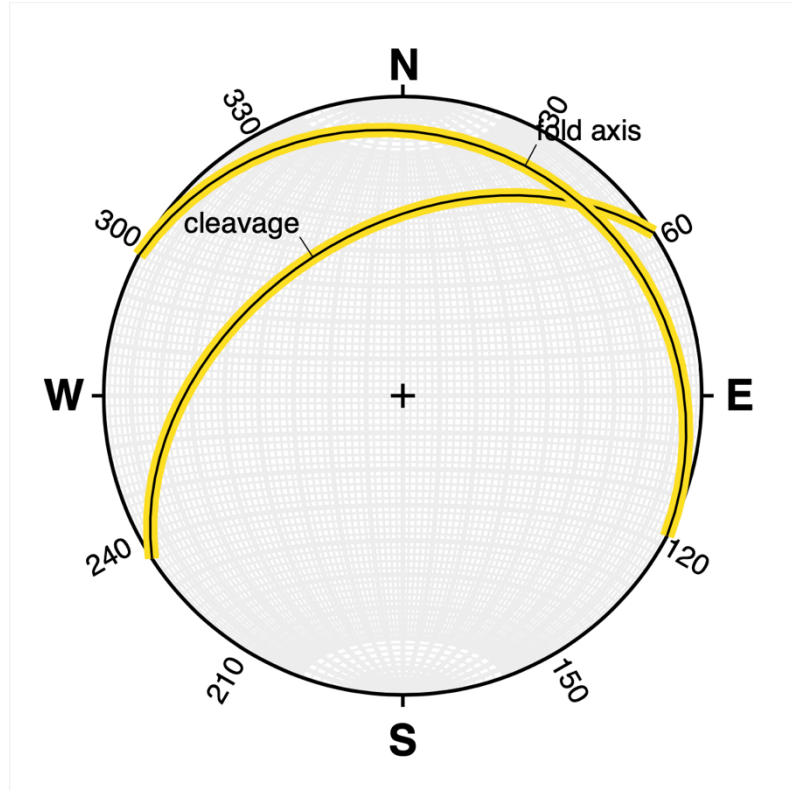


Figure 15. Fracture with crushed mica (M) along one border, in PPL (left) and XPL (left). Otherwise, either side of the fracture shows a groundmass of quartz and mica.

mostly empty space. Some locations within the fracture showed undulate extinction in XPL, suggesting that it could contain quartz. SEM spectral analysis, however, revealed certain differences in elemental composition for small circular or oval masses within the fracture (Appendix B, Figure 1). The fracture branches off several times within the slide. The folding within the sample ranges from larger, following the fabric outlined in Figure 7 to smaller fold structures found throughout the sample.

3.3 SEM Elemental Analysis

These grains returned elemental spectra through SEM analysis. In total, 65 points were analyzed throughout the whole thin section. The quartz grains returned peaks at Si and O under spectral analysis, in agreement with our earlier analysis. Analysis of the larger grains with first-order birefringence revealed peaks at Ca, C, O, Mn, Fe, Si, Mg, Al, and Yb. The longer, rectangular grains showed peaks at Ca, Si, Al, Fe and Mg. When the micas were targeted, they showed a multitude of different elements that differed somewhat between grains, but included Si, Al, O, Mg, Fe, Ti, K. The spectral analysis of the square/triangular metallic grains revealed peaks at Fe and S. Interestingly enough, when points were taken in the center of the grain, they returned Fe and S, but points from the edges of the grain came back with peaks at Fe and O, with varying peaks of Si, Ca, and S. The SEM picked up peaks of a few rare earth elements such as Yb (larger grains) and La (in the square metallic grains). SEM elemental analysis graphs and accompanying images can be found in Appendix B.

4. Discussion

This section will discuss the compiled results and interpret them according to the data collected. The minerals will be named based on their properties as listed in the results, and textures will be discussed. Next, the evidence for deformation will be related to structures observed, and the stages of deformation will be sorted by most recent to least recent. Based on the work conducted and evaluation of the previous literature, an environment of formation will be discussed. Future work would include expanding the project geographically, to include other samples within the YTT and adjacent terranes to determine if stages of deformation are drastically different. This would benefit the mapping of the area and future studies regarding terrane accretion and deformation history.

4.1 Mineralogy

Based on results from the SEM and the petrographic microscope, it is concluded that the round grains in the matrix are quartz (Fig. 8). Some areas of quartz grains are elongated in one direction and show continuous undulate extinction, suggesting they experienced low strain during plastic deformation (Blenkinsop, 2007). This shape preferred orientation is a characteristic of intracrystalline plasticity (Blenkinsop, 2007). The mica mass is interpreted to contain muscovite and chlorite. Any other possible mica minerals in the groundmass are too fine-grained to

identify. It is worth noting that the two identifiable micas are hard to completely separate, as they frequently occupy the same space within the thin section. Because of how the quartz and mica occupy the same space, with no obvious indication otherwise, it is assumed that they both crystallized around the same time. It is possible to see individual examples of muscovite and chlorite, but when it comes to SEM analysis, for example, the two are frequently mixed together. This could be why the SEM data for the micas returned such a variety of elements. The chlorite could also be why the rock looks green to the naked eye. Chlorite can form from the alteration of mafic minerals such as pyroxenes. The rectangular grains (shown in Figure 11) are assumed to be pyroxenes, due to their cleavage and fracture patterns. One of these pyroxene grains was observed to overprint a kinked muscovite, which gives evidence for the possibility that the pyroxenes crystallized after the muscovite and quartz in this sample. The larger grains with first order to low second order birefringence were determined to be carbonates, likely calcite or a similar polymorph. This was also due to the characteristic twinning patterns, with twin sizes ranging from < 1 micron to 5 microns. Twin size can have a correlation with its temperature during deformation (Brandstätter et al., 2007). The twinning of the calcite points to those grains being deformed in an environment with temperature lower than 400 °C (Ferrill et al., 2004) (Brandstätter et al., 2007). It is hard to predict when they formed because of a lack of overprinted grains or similar evidence. All of the quartz, micas and carbonates were crystallized prior to the folding event, because of their position within the differentiated layers. The metallic grains were labeled as pyrite, because of their habit and given that the SEM analysis reliably demonstrated spectral peaks at Fe and S. This was also based on visible grains in the rock. These formed after the folding, since they are found all throughout the sample without any distinction in area. Attempts to isolate points of the rust-colored fine-grained mineral for SEM spectral analysis returned many different elements per grain and thus the analysis was inconclusive beyond classification as an oxidation product. For clarification, the rust was found all over the thin section, and affected most calcite grains, so the spectral analysis could not return specific elements to the rust alone.

4.2 Evolution

Due to the stages of deformation and alteration, it is difficult to estimate the protolith of this rock. Minerals like muscovite and chlorite are likely products of alteration, which leaves the quartz, pyroxenes, and carbonates. Mineral alteration throughout the slide, as shown in Figure

13, mainly targets the calcite grains. A remarkable observation from Figure 13 shows the alteration passing through the middle of the grain but nowhere else, leaving the shape of the grain intact other than the middle section. This alteration shows a rusty colour in the hand sample and in thin section. There are at least 3 stages of deformation. The newest and latest stage of deformation is ductile deformation evident in the folding of the sample, on large scale within the outcrop shown in Figure 5a, but also a smaller microscale within the thin section (Fig. 7). This may be related to the kinking of the mica (Fig. 11), however, if it is not, then the kinking and the fracture in the slide could be evidence of a brittle deformation event (Scholtz and Choi, 2022). The mica kinking could also be linked to a slipping movement related to ductile shear (Bell et al., 1986). A shear deformation event is supported by the crushed mica along the one side of the fracture, as shown in Figure 15. A third stage of deformation was identified in the field. Lineations were observed on the surface of the fold, meaning that the sample underwent ductile deformation and was foliated prior to the latest folding event. This is the oldest of the deformation stages. Either of the ductile deformation events could have been the cause of the intracrystalline plasticity that caused the calcite twinning, quartz undulatory extinction, quartz preferred orientation, and some of the mica kinking (Blenkinsop, 2007). Both of our ductile deformation stages can be compared to events recorded by Mihalynuk et al. (2006). Mihalynuk et al. (2006) mentions a stage of orogeny deformation, which could relate to our first ductile deformation event interpreted from the foliation on the fold surface. Mihalynuk et al. (2006) also states that the last stage of deformation is folding correlated to a rapid uplift event, which could correspond with our last interpreted stage of ductile folding. This rapid uplift event is related to collision with the northern continental margin (Mihalynuk et al., 2006) which would be pre-Jurassic and fit with the observation of Moynihan et al. (2022) that no post-Jurassic rocks are deformed, with the exception of a few during the transition period. Moynihan et al. (2022) found that all pre-Jurassic rocks in this region were deformed, but any younger rocks were not, with the exception of some intermediary early Jurassic stage intrusions. Our sample is deformed; therefore, it is definitely pre-Jurassic. However, given that it was found within the YTT region recently mapped by Moynihan et al. (2022) and is likely part of the Slate Mountain succession, it is interpreted to be of Mississippian age. In following with the environment of formation of the YTT in which this sample was found, we can assume that it was formed in a volcanic back-arc setting.

It is hard to determine the environment of temperature and pressure that led to stages of deformation in this rock, given that the minerals it contains are common. If the chlorite formed during regional metamorphism, then its presence in this greenschist facies suggests that the temperature during that stage of metamorphism ranged from 350-500 °C (Parra et al., 2002), with low pressure. Evidence for low pressure metamorphism in our sample differs from prior work like that of Creaser et al. (1997) detailing possible evidence for high pressure metamorphism in the Big Salmon Range. The evidence discussed in the work described the morphology and geochemistry of zircons dated from an eclogite within the YTT. However, de Keijzer et al. (1999) states that the evidence for high pressure metamorphism is found only in isolated lenses, with little documented evidence. Zircons were not observed during petrographic analysis, and the proposed evidence for high pressure metamorphism was not identified in our sample.

Because of a lack of metamorphic index minerals other than chlorite, it can be assumed that this sample is low to medium grade. As mentioned at the beginning of this section, it is hard to isolate the protolith from the current rock by looking only at this one sample. Continuity and the scale of observation will influence how these microstructures are interpreted. Observations made over a greater distance would help with clarity as to whether the rock is metasedimentary or meta-igneous based on how the facies and deformation changes. However, given its location northeast of the Little Bear fault and staying consistent with prior work (Moynihan et al., 2022) it is likely the sample is meta-igneous.

Conclusions

The orientated sample was analysed via petrographic and SEM methods, and it was concluded that the main minerals present in the thin section were the quartz-muscovite-chlorite bands interspersed by the clusters of calcite-carbonates and pyroxene grains. The specimen is a concentrically folded, meta-igneous greenschist unit which has clearly undergone at least three stages of deformation, a characteristic of the YTT. The oldest stage was the ductile deformation event that led to the foliation that was seen on the surface of the fold. A second stage of brittle deformation can be interpreted from the features like the fracture and mica kinking. A third stage was the deformation that caused the folding that is so evident in our sample outcrop. The sample is estimated to be Mississippian in age, with its last major deformation event taking place before

the Jurassic period, based on the latest ductile deformation and area in which it was found, north of the Little Bear fault (Moynihan et al., 2022). This sample was likely formed in a volcanic back-arc system and at one point, metamorphosed regionally at relatively shallow crustal depths with low to moderate pressure and 350-500 °C temperatures. If you consider the findings of Brandstätter et al. (2007) and Ferrill et al. (2004) based on calcite deformation twins, the temperature range can be whittled down to a range of 350-400 °C. This fits with the evolution of the region, given that this part of the Yukon territory is interpreted to comprise accreted island arcs which underwent orogenic and collisional events during the Late Paleozoic-Early Mesozoic (Mihalynuk et al., 2006). The evidence for ductile deformation is strong both within the sample and in the literature. Hansen et al. (1991) states that the YTT formed from deformed ductile tectonites. The mineralogical and structural evidence also agree with the previous works, including de Keijzer et al. (1999), when it comes to the lack of evidence for high pressure metamorphism in this particular area.

Future work in this study would consist of expanding the sampling region geographically, to include other outcrops in nearby units and even neighboring terranes. Given that we have an oriented sample, we could compare the foliation and other measurements with surrounding lithologies to estimate how representative our sample is of the area. Examination and comparison of our sample to others could help define limits to mappable units, which only increases the amount of usable, public data, which has implications for further research in the YTT and possible mineral exploration.

References

- Bell, I.A., Wilson, C.J.L., McLaren, A.C., Etheridge, M.A. (1986) Kinks in mica: Role of dislocations and (001) cleavage. In *Tectonophysics*, 127(1–2), 49-65. ISSN 0040-1951.
- Blenkinsop, T. G. (2007). *Deformation microstructures and mechanisms in minerals and rocks*. Springer Science & Business Media.
- Brandstätter, J., Kurz, W., & Rogowitz, A. (2017). Microstructural analysis and calcite piezometry on hydrothermal veins: Insights into the deformation history of the Cocos Plate at Site U1414 (IODP Expedition 344). *Tectonics*, 36(8), 1562-1579.
- Chakrabarti, K., Eeka, N.R.R., Mishra, B., Kumar, K.M., Katti, V.J., Umamaheswar, K., Parihar, P.S., Mukhopadhyay, J. and Ghosh, G., 2013. Gold, silver and platinum group of elements mineralization in Precambrian uraniferous quartz-pebble conglomerates of Mankarhachua area, Angul District, Odisha. *Current Science*, pp.978-983.
- Churkin Jr, M., Foster, H. L., Chapman, R. M., & Weber, F. R. (1982). Terranes and suture zones in east central Alaska. *Journal of Geophysical Research: Solid Earth*, 87(B5), 3718-3730.
- Colpron, M. (2005). Geology and mineral potential of Yukon-Tanana Terrane in the Livingstone Creek area (NTS 105E/8), south-central Yukon. *Yukon Exploration and Geology*, 93-107.
- Colpron, M., Nelson, J. L., & Murphy, D. C. (2007). Northern Cordilleran terranes and their interactions through time. *GSA today*, 17(4/5), 4.
- Creaser, R. A., Heaman, L. M., & Erdmer, P. (1997). Timing of high-pressure metamorphism in the Yukon-Tanana terrane, Canadian Cordillera: constraints from U-Pb zircon dating of eclogite from the Teslin tectonic zone 1 ~.
- de Keijzer, M. (2002). Tectonic evolution of the Teslin zone and the western Cassiar terrane, northern Canadian cordillera.
- de Keijzer, M., Williams, P. F., & Brown, R. L. (1999). Kilometre-scale folding in the Teslin zone, northern Canadian Cordillera, and its tectonic implications for the accretion of the Yukon-Tanana terrane to North America 1.
- Du, G., Wang, K., Ran, J., Wang, F., Pan, Z. (2014). Application of IR/SEM and Other Modern Instruments for Mineral Identification. *Rock and Mineral Analysis*, 33(5): 625 -633.

- Ferrill, D. A., Morris, A. P., Evans, M. A., Burkhard, M., Groshong Jr, R. H., & Onasch, C. M. (2004). Calcite twin morphology: a low-temperature deformation geothermometer. *Journal of structural Geology*, 26(8), 1521-1529.
- Hansen, V. L. (1989). Structural and kinematic evolution of the Teslin suture zone, Yukon: record of an ancient transpressional margin. In *Journal of Structural Geology* (Vol. 11, Issue 6).
- Hansen, V. L., Heizler I, M. T., & Mark Harrison, T. I. (1991). Mesozoic thermal evolution of the Yukon-Tanana composite terrane: new evidence from $^{40}\text{Ar}/^{39}\text{Ar}$ data. In *TECTONICS* (Vol. 10, Issue 1).
- Humayun, M., Nemchin, A., Zanda, B., Hewins, R.H., Grange, M., Kennedy, A., Lorand, J.P., Göpel, C., Fieni, C., Pont, S. and Deldicque, D., 2013. Origin and age of the earliest Martian crust from meteorite NWA 7533. *Nature*, 503(7477), pp.513-516.
- Mihalynuk, M. G., Friedman, R. M., Devine, F., Heaman, L. M., Colpron, M., & Nelson, J. L. (2006). Protolith age and deformation history of the Big Salmon complex, relicts of a Paleozoic continental arc in northern British Columbia. *Paleozoic Evolution and Metallogeny of Pericratonic Terranes at the Ancient Pacific Margin of North America, Canadian and Alaska Cordillera: Geological Association of Canada Special Paper*, 45, 179-200.
- Moynihan, D., Crowley, J. L., & And Crowley, J. L. (2022). Preliminary observations on the geology of the southern Big Salmon Range, south-central Yukon (parts of NTS 105C/13, 14, 105F/4 and 105E/1). In *Yukon Geological Research Yukon Exploration and Geology*.
- Murphy, D. C., Mortensen, J. K., Piercey, S. J., Orchard, M. J., Gehrels, G. E., Colpron, M., & Nelson, J. L. (2006). Mid-Paleozoic to early Mesozoic tectonostratigraphic evolution of Yukon-Tanana and Slide Mountain terranes and affiliated overlap assemblages, Finlayson Lake massive sulphide district, southeastern Yukon. *Paleozoic evolution and metallogeny of pericratonic terranes at the ancient Pacific margin of North America, Canadian and Alaskan Cordillera: Geological Association of Canada Special Paper*, 45, 75-105.
- Parra, T., Vidal, O., & Jolivet, L. (2002). Relation between the intensity of deformation and retrogression in blueschist metapelites of Tinos Island (Greece) evidenced by chlorite–mica local equilibria. *Lithos*, 63(1-2), 41-66.
- Parsons, A. J., McClelland, W. C., Zagorevski, A., Ryan, J. J., Coleman, M. J., Cleven, N., & van Staal, C. R. (2022). U-Pb zircon geochronology from the Northern Cordillera, central Yukon, with implications for its tectonic assembly. *Tectonics*, e2021TC006918.

- Scholz, C. H., & Choi, E. (2022). What comes first: The fault or the ductile shear zone?. *Earth and Planetary Science Letters*, 577, 117273.
- Ruks, T. W., Piercey, S. J., Ryan, J. J., Villeneuve, M. E., & Creaser, R. A. (2006). Mid-to late Paleozoic K-feldspar augen granitoids of the Yukon-Tanana terrane, Yukon, Canada: Implications for crustal growth and tectonic evolution of the northern Cordillera. *Geological Society of America Bulletin*, 118(9-10), 1212-1231.
- Simard, R. L., Dostal, J., & Roots, C. F. (2003). Development of late Paleozoic volcanic arcs in the Canadian Cordillera: an example from the Klinkit Group, northern British Columbia and southern Yukon. *Canadian Journal of Earth Sciences*, 40(7), 907-924.
- Stevens, R. A., & Erdmer, P. (1996). Structural divergence and transpression in the Teslin tectonic zone, southern Yukon Territory. *Tectonics*, 15(6), 1342–1363.
<https://doi.org/10.1029/96TC01134>
- Stevens, R. A. (1997). Structural and tectonic evolution of the Teslin tectonic zone, Yukon: A doubly-vergent transpressive shear zone.
- Templeman-Kluit, D.J., (1984) *Geology, Laberge (105E) and Carmacks (105I), Yukon Territory*, Geological Survey of Canada, Open File Report 1101, 1:250 000 scale.
- Tomomewo, O. S., Jabbari, H., Badrouchi, N., Onwumelu, C., & Mann, M. (2019, June). Characterization of the Bakken Formation using NMR and SEM Techniques. In 53rd US Rock Mechanics/Geomechanics Symposium. OnePetro.

Appendix A

(a)

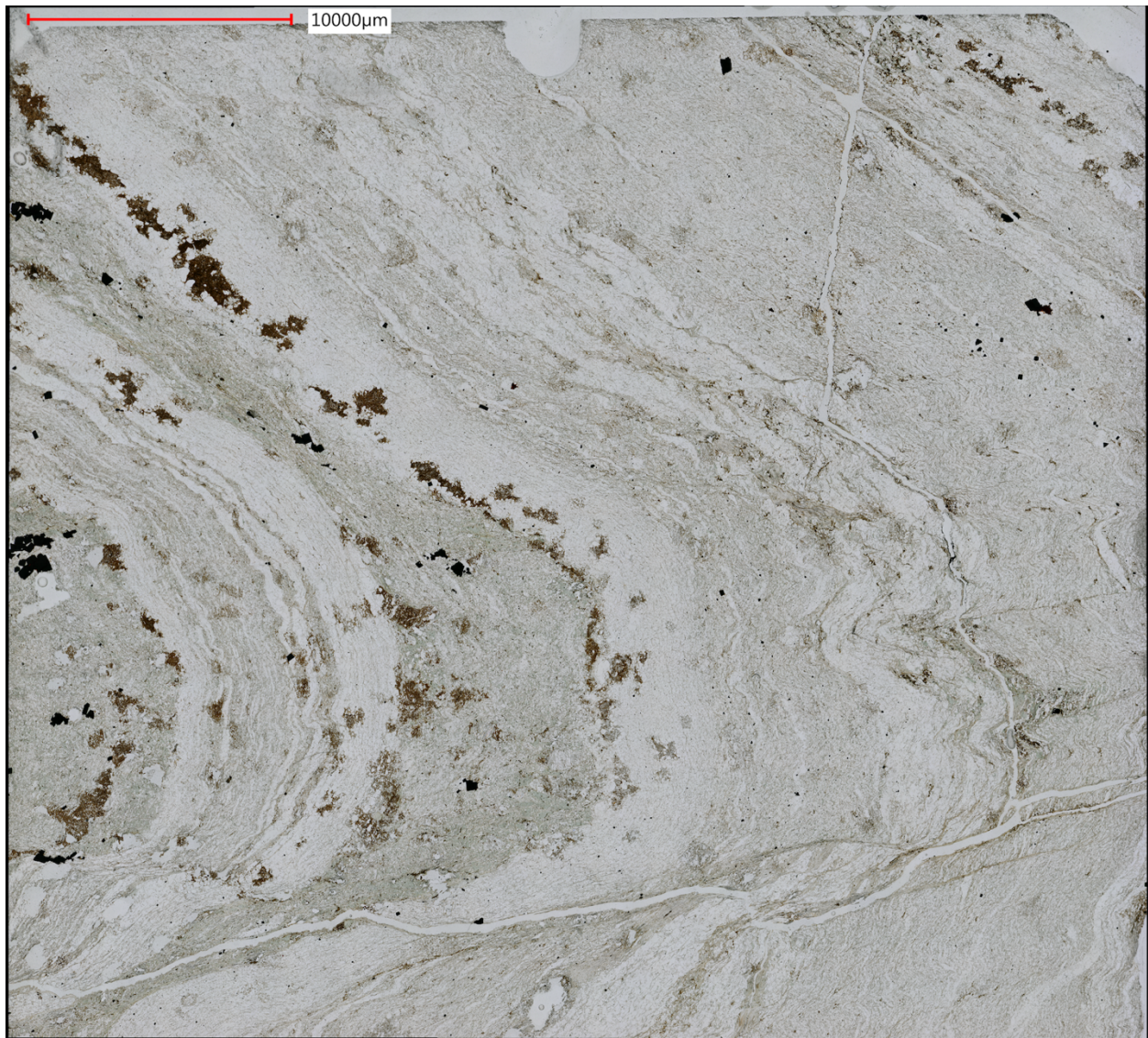


Figure A1. (a) First half-slide scan in PPL. Groundmass is mostly quartz and muscovite, which is why it is clear in PPL. Some of the larger, dark grains are pyroxene and some may also be calcite grains that are being altered, leading to them seeming rusty-coloured in thin section. **(b)** First half-slide scan in XPL. **(c)** Second half-slide scan in PPL. **(d)** Second half-slide scan in XPL.

(b)

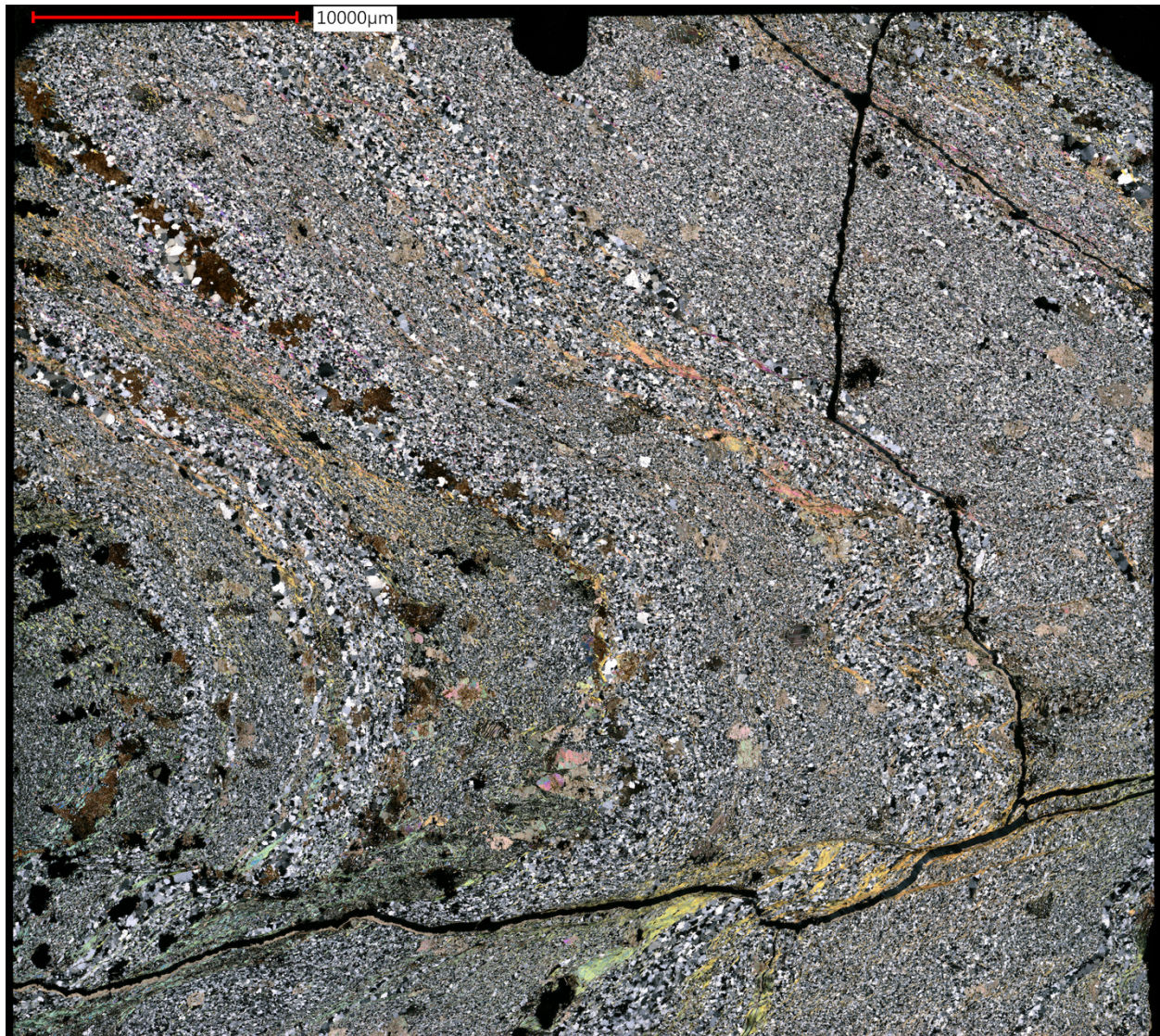


Figure A1. (b) Large grains are calcite. Groundmass is mostly quartz, muscovite, and chlorite. Fracture runs along at bottom and to the right side of image. Some dark grains may be pyrite, but they may also be some other mineral that is extinct at this particular angle, or empty space. Moderate range of grain sizes on this half of the slide.

(c)



Figure A1. (c) Groundmass is mostly quartz and muscovite, which is why it is clear in PPL. Some of the larger, dark grains are pyroxene and some may also be calcite grains that are being altered, leading to them looking rusty-coloured in thin section.

(d)

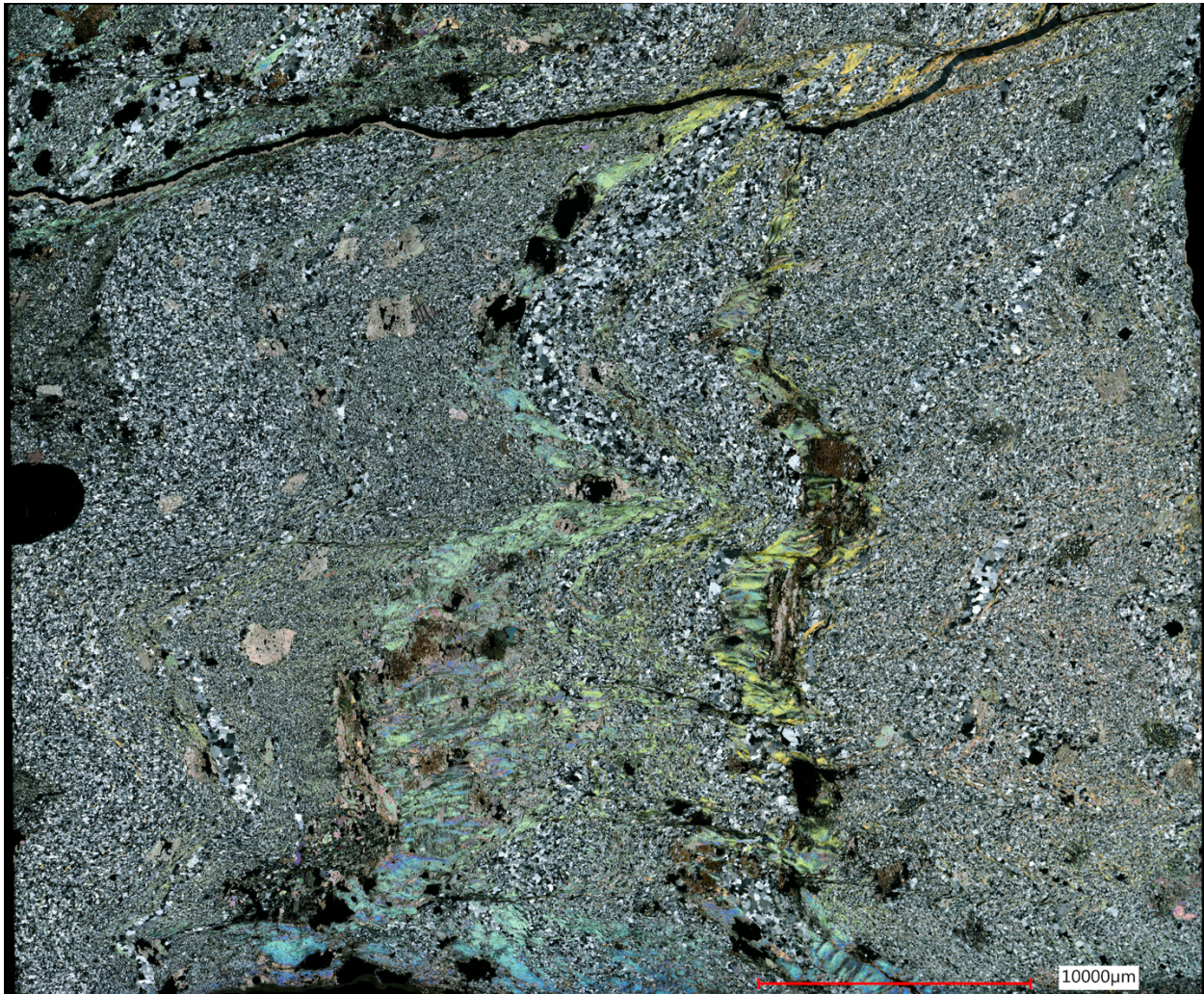
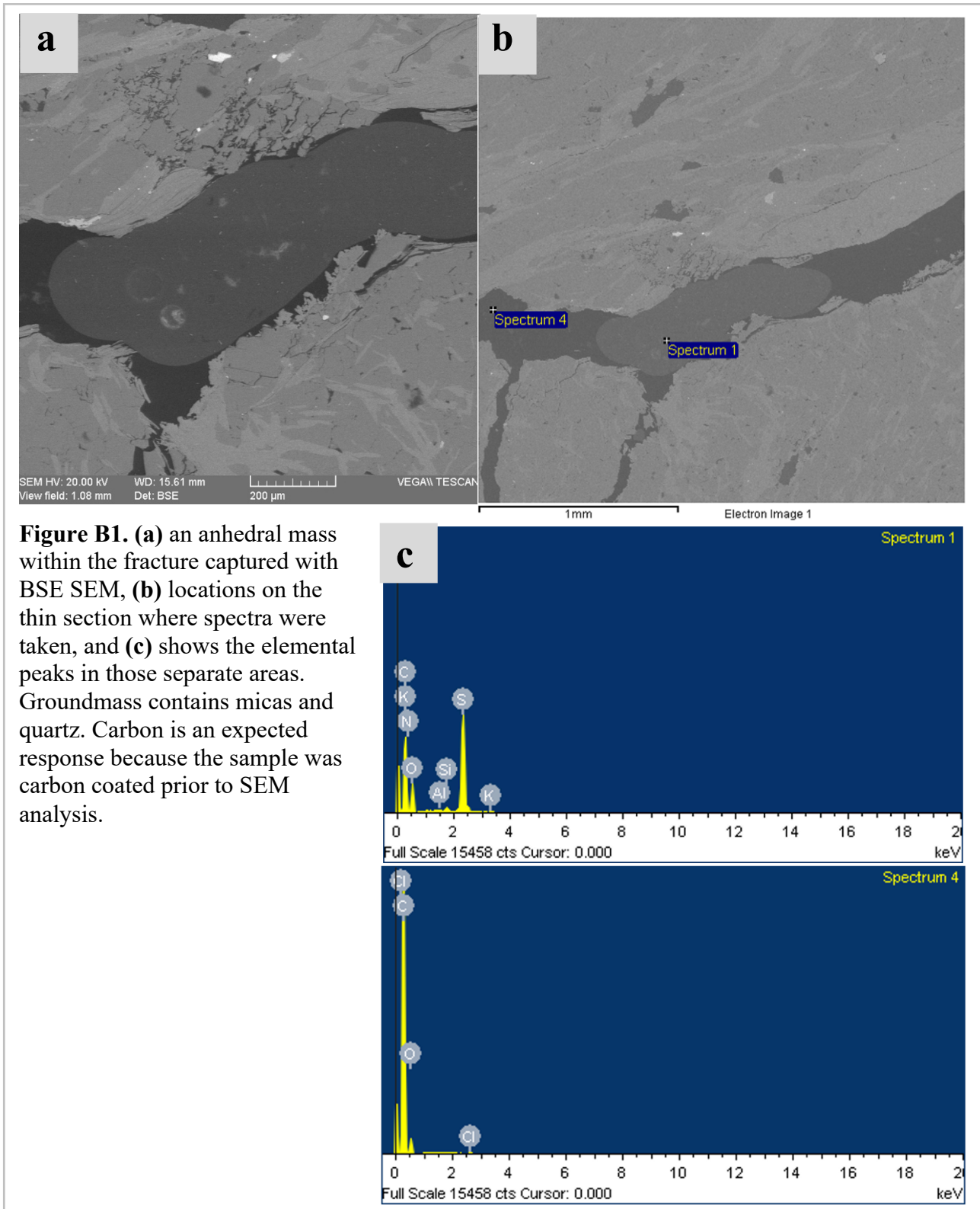


Figure A1. (d) Large grains are calcite. Groundmass is mostly quartz, muscovite, and chlorite. Bands of deformed muscovite can be seen with their high order birefringence colours. Fracture runs along at top of image. Some dark grains may be pyrite, but they may also be some other mineral that is extinct at this particular angle. Wider range of grain sizes on this half of the slide.

Appendix B

All figures in this section will comprise of a SEM image and its corresponding SEM BSE spectral analysis chart, showing peaks at the dominant elements.



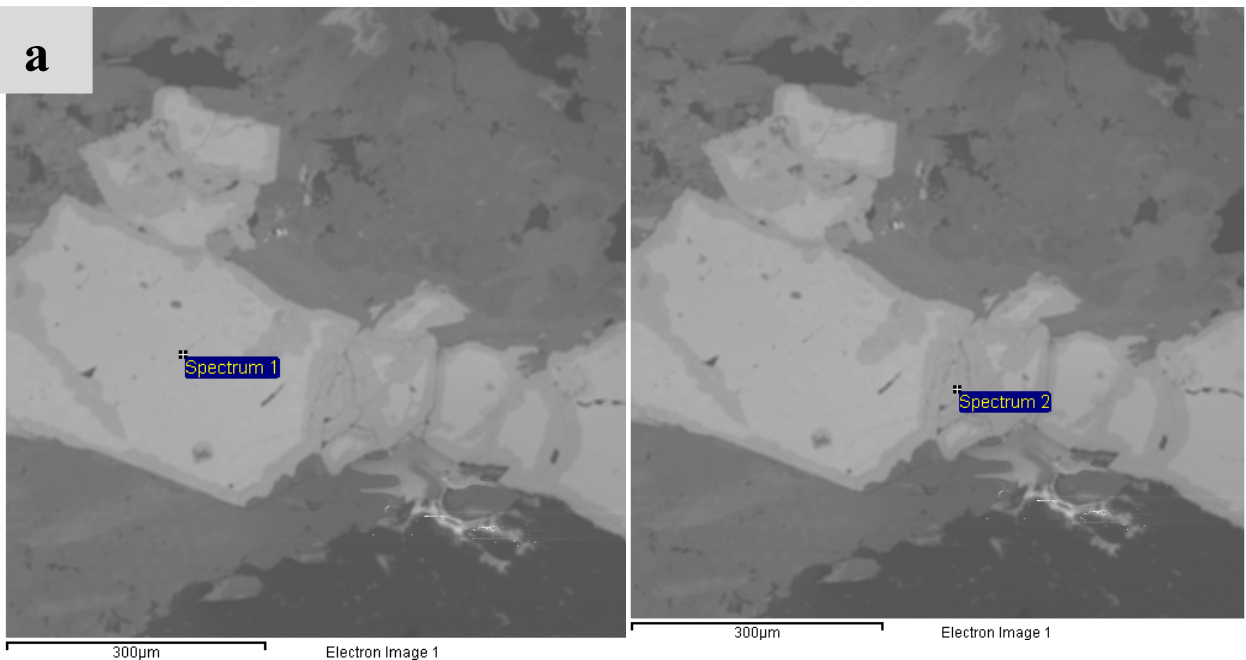
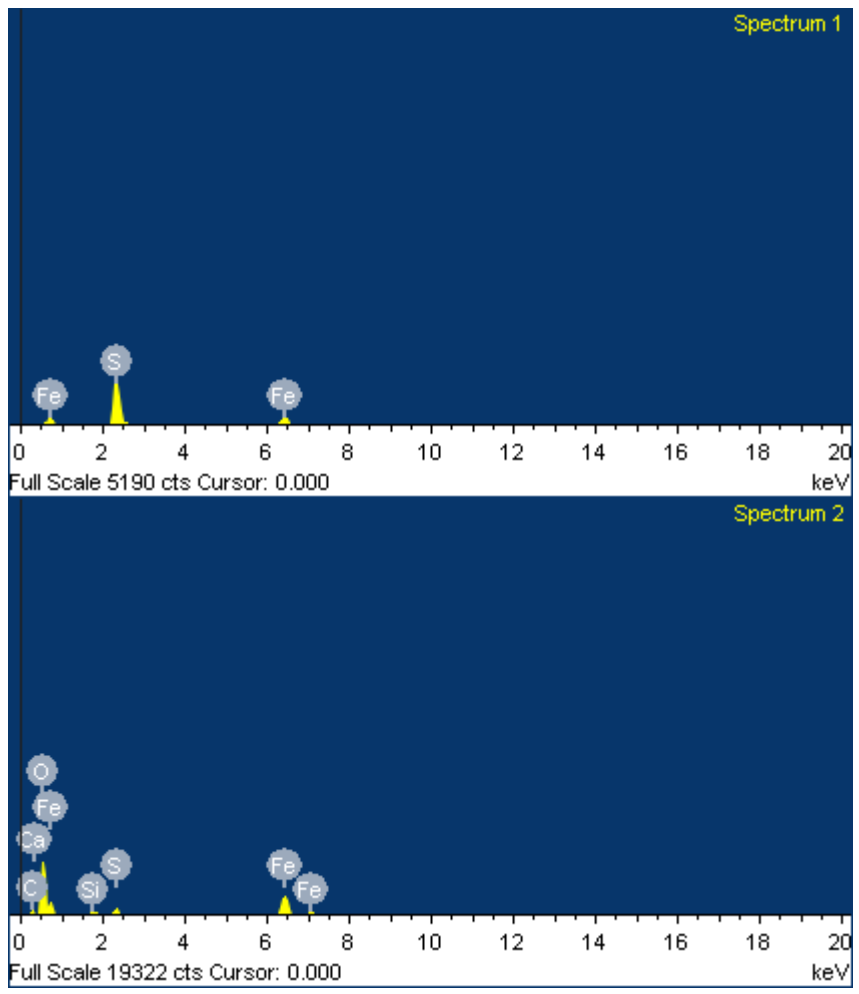


Figure B2. (a) Pyrite grain surrounded by a groundmass of quartz and mica. Notice the different composition in the outward zone of the grain. (b) This pyrite grain returned a peak at La (Lanthanum). (c) A second point showing a different group of elements in the outer zone of the pyrite grain.



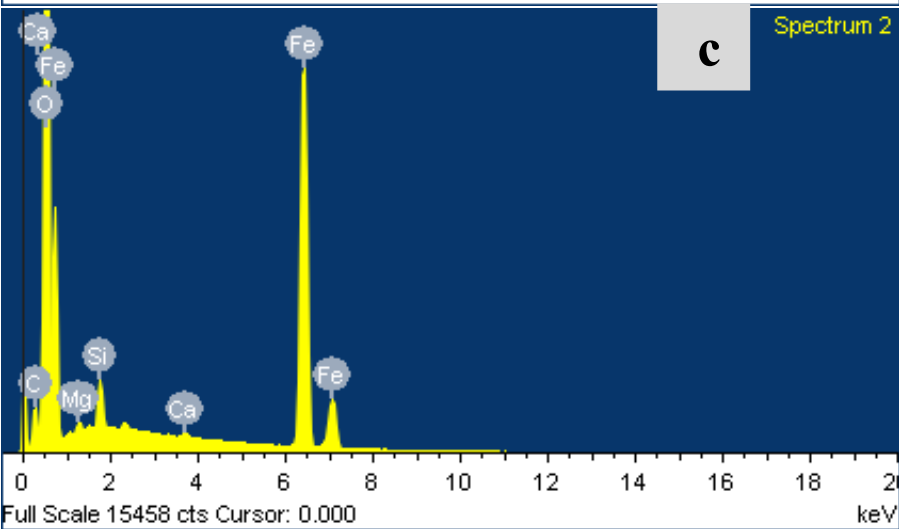
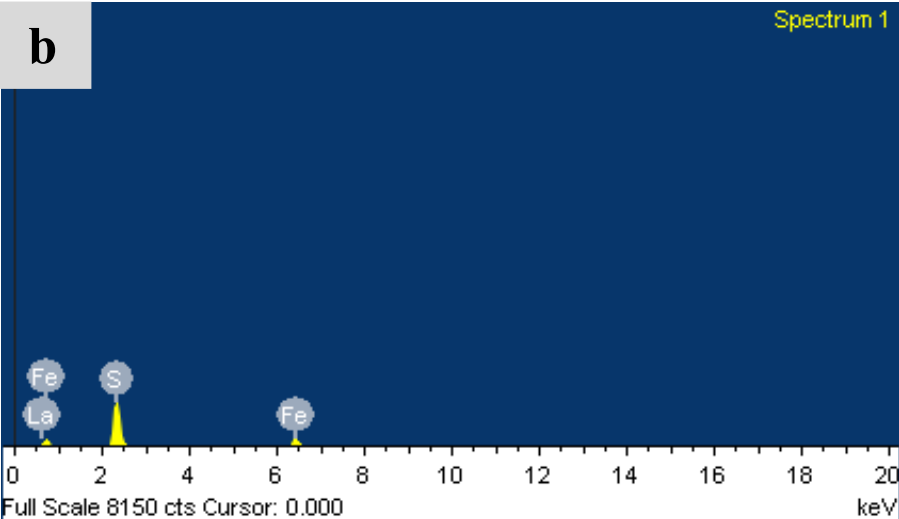
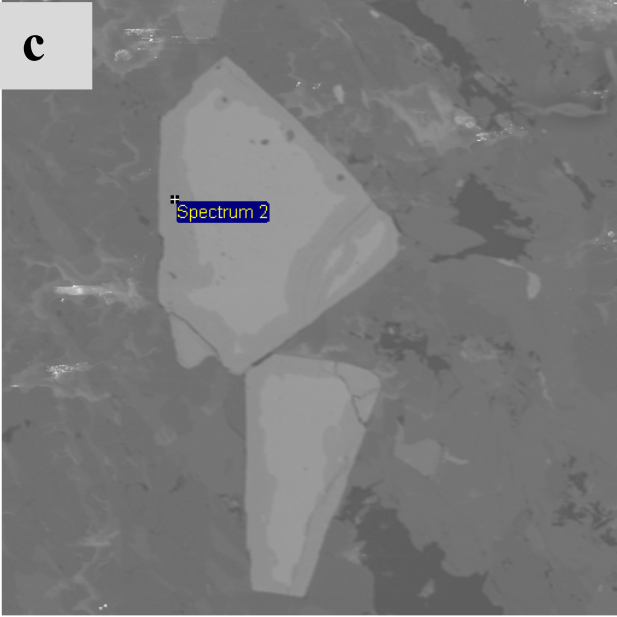
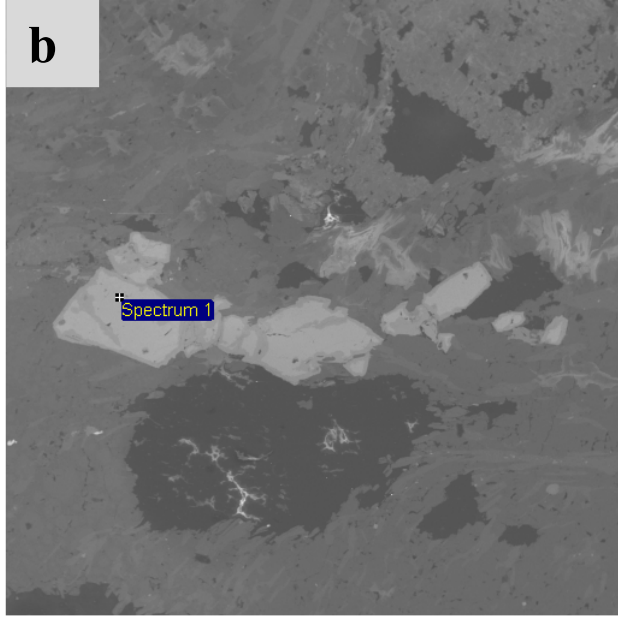


Figure B3. Pyroxene grain, long and rectangular, lightly outlined in yellow. The colour is not contrasted well from the background due to the resemblance in elements making up the mica groundmass and the pyroxene grain. The light streaks covering some of the grain is interference due to contrasting magnetic fields. Chart showing elemental percentages detected below.

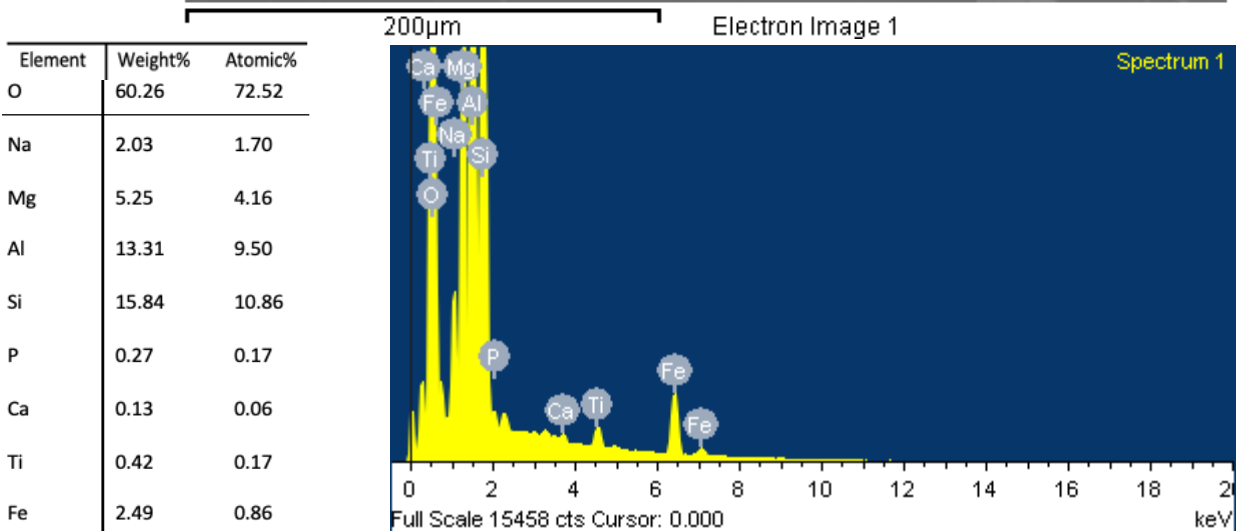
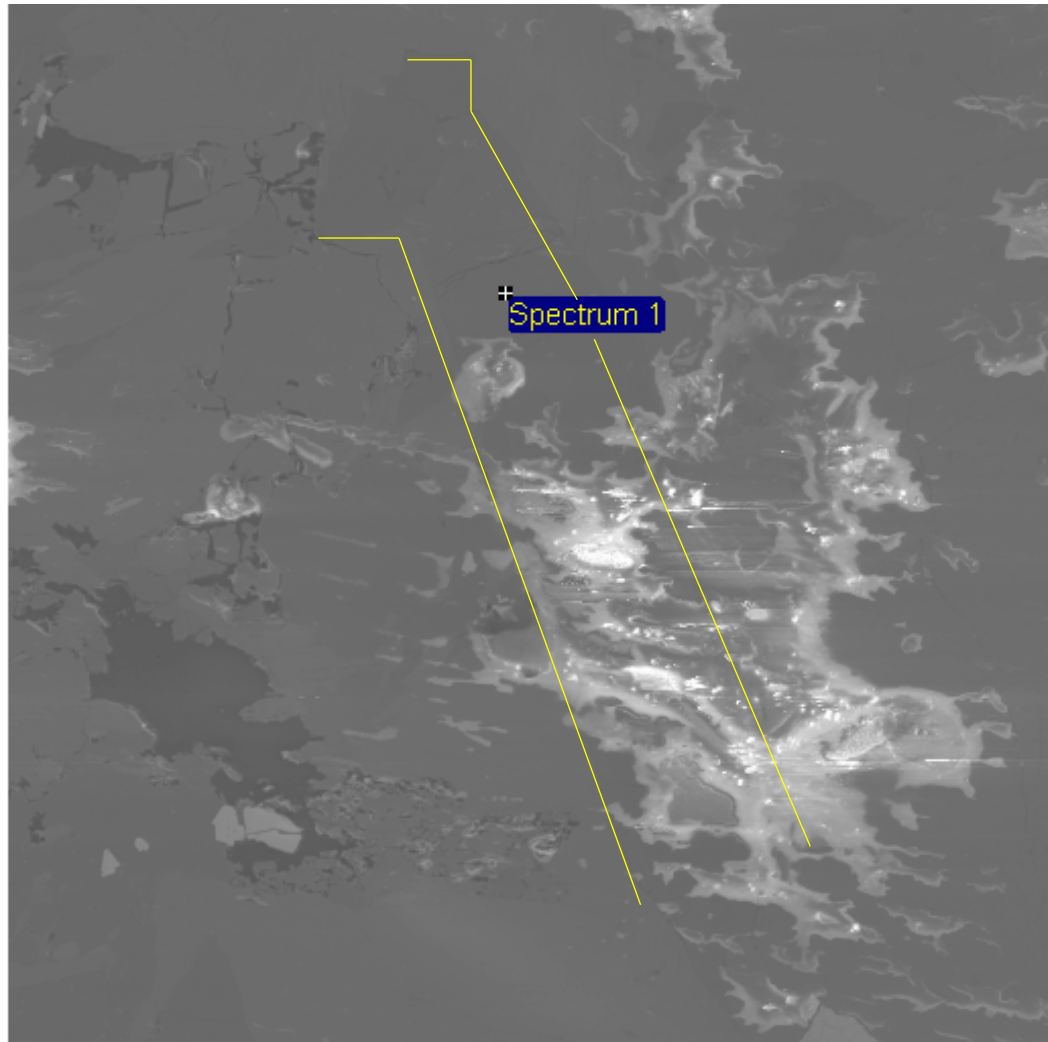


Figure B4. Calcite grains and their corresponding SEM BSE charts in **(a)** and **(b)**. Notice that **(b)** shows a peak at Ytterbium.

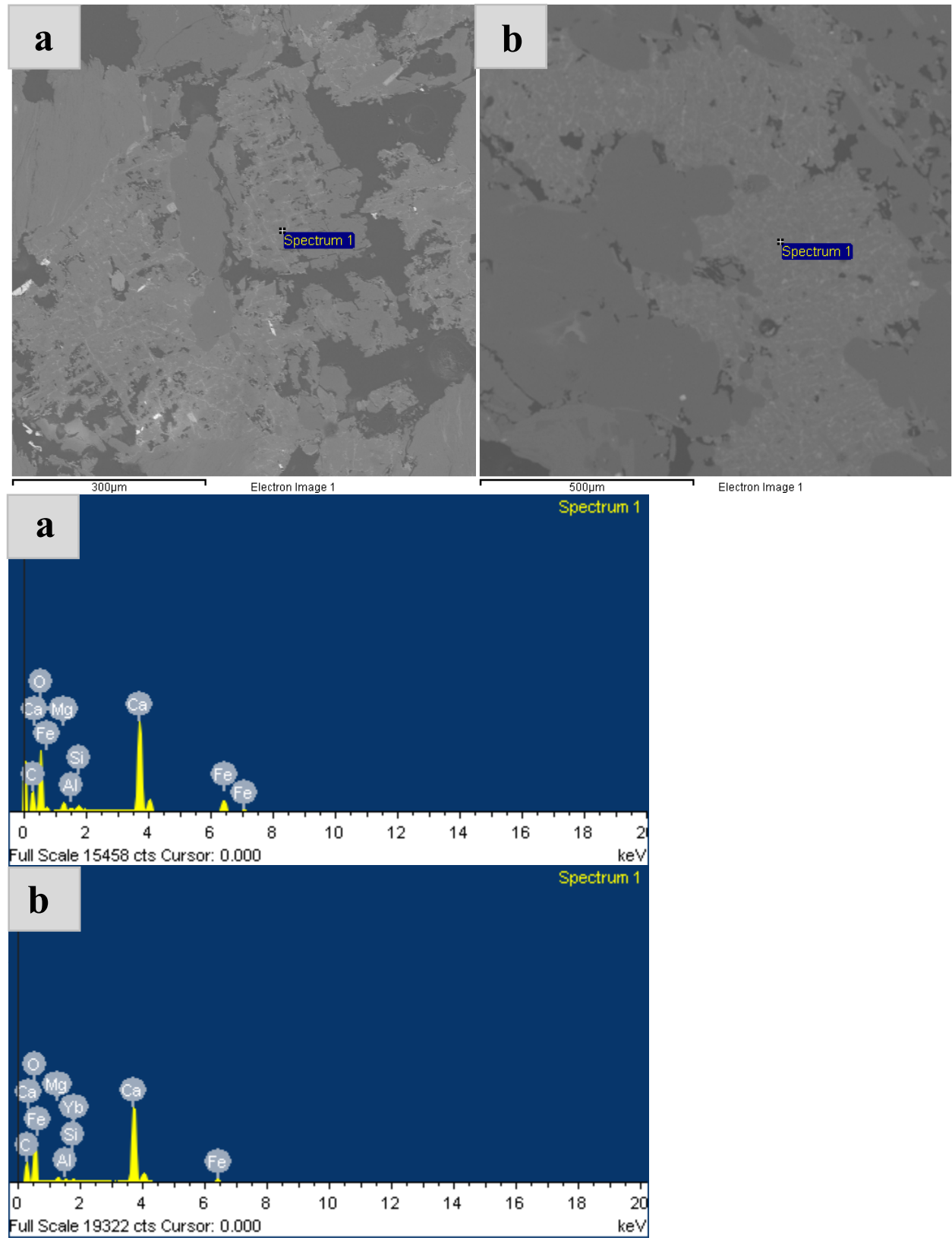


Figure B5. Quartz grains and corresponding chart, showing very clear peaks at Si and O. The peak at C is expected because the thin section was carbon coated before being examined by SEM.

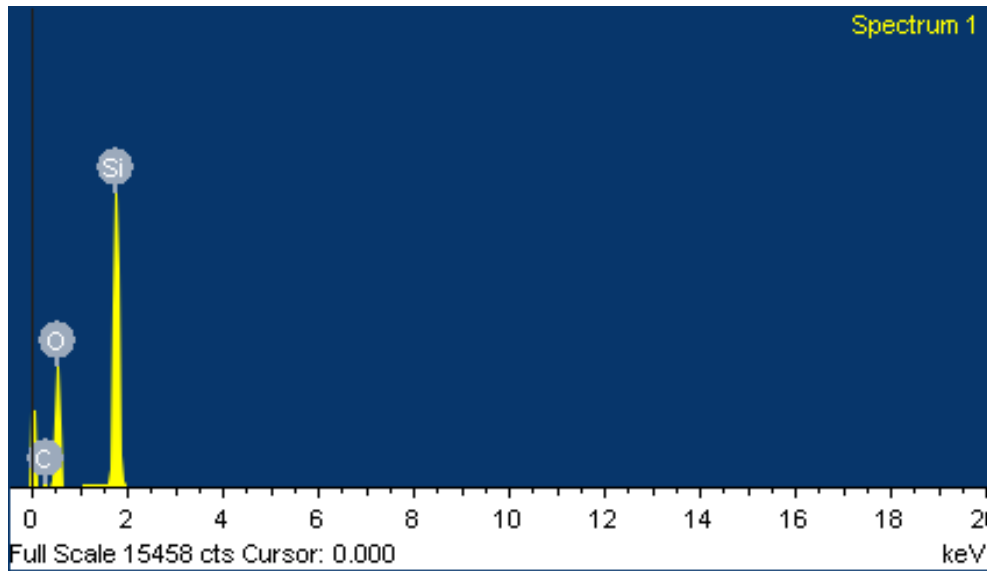
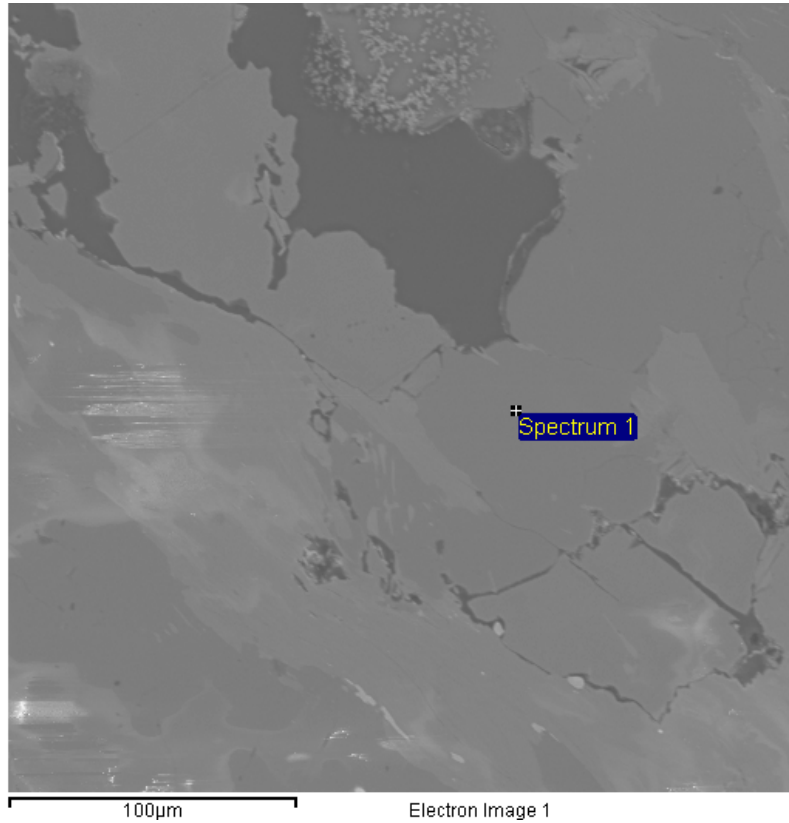


Figure B6. Mixed micas and the corresponding chart. The muscovite and chlorite were too intermixed to be able to accurately separate them for the purpose of this analysis.

